

FIRST-based survey of Compact Steep Spectrum sources

III. MERLIN and VLBI observations of subarcsecond-scale objects

A. Marecki¹, M. Kunert-Bajraszewska¹, and R. E. Spencer²

¹ Toruń Centre for Astronomy, N. Copernicus University, 87-100 Toruń, Poland

² Jodrell Bank Observatory, The University of Manchester, Macclesfield, Cheshire, SK11 9DL, UK

Received 27 June 2005 / Accepted 25 November 2005

ABSTRACT

Context. According to a generally accepted paradigm, small intrinsic sizes of Compact Steep Spectrum (CSS) radio sources are a direct consequence of their youth, but in later stages of their evolution they are believed to become large-scale sources. However, this notion was established mainly for strong CSS sources.

Aims. In this series of papers we test this paradigm on 60 weaker objects selected from the VLA FIRST survey. They have 5-GHz flux densities in the range $150 < S_{5\text{GHz}} < 550$ mJy and steep spectra in the range $0.365 \leq \nu \leq 5$ GHz. The present paper is focused on sources that fulfill the above criteria and have angular sizes in the range $\sim 0''.2 - 1''$.

Methods. Observations of 19 such sources were obtained using MERLIN in “snapshot” mode at 5 GHz. They are presented along with 1.7-GHz VLBA and 5-GHz EVN follow-up snapshot observations made for the majority of them. For one of the sources in this subsample, 1123+340, a full-track 5-GHz EVN observation was also carried out.

Results. This study provides an important element to the standard theory of CSS sources, namely that in a number of them the activity of their host galaxies probably switched off quite recently and their further growth has been stopped because of that. In the case of 1123+340, the relic of a compact “dead source” is particularly well preserved by the presence of intracluster medium of the putative cluster of galaxies surrounding it.

Conclusions. The observed overabundance of compact sources can readily be explained in the framework of the scenario of “premature” cessation of the activity of the host galaxy nucleus. It could also explain the relatively low radio flux densities of many such sources and, in a few cases, their peculiar, asymmetric morphologies. We propose a new interpretation of such asymmetries based on the light-travel time argument.

Key words. Radio continuum: galaxies, Galaxies: active, Galaxies: evolution

1. Introduction

Following the first paper defining the class of Compact Steep Spectrum (CSS) sources (Peacock & Wall, 1982), two almost identical surveys of CSS sources (Spencer et al., 1989; Fanti et al., 1990) based on the 3CR catalogue and the Peacock & Wall (1982) list have been constructed. CSS sources collected in these samples – they are often labelled jointly as the so-called 3CRPW sample – are as powerful as large-scale Fanaroff-Riley type II (FR II, Fanaroff & Riley, 1974) radio sources, yet their angular sizes are of the order of a few arcseconds. Their interpretation was given by Fanti et al. (1990) and has become a paradigm (see O’Dea, 1998, for a review). According to this paradigm, the large majority of CSS sources are intrinsically small objects – their true linear sizes

are $\lesssim 20h^{-1} \text{ kpc}^1$ – so that their small angular sizes do not result from projection.

As their linear sizes are subgalactic, CSS sources are immersed in their host galaxies and it is obvious that the environment responsible for the observable effects, such as strong and often asymmetric depolarisation of the radio emission caused by Faraday rotation (Saikia et al., 1985, 1987; Akujor & Garrington, 1995; Lüdke et al., 1998; Fanti et al., 2004), must have an influence on morphologies and the evolution of CSS sources. A strong interaction with the host galaxy

¹ For consistency with earlier papers in this field, the following cosmological parameters have been adopted throughout this paper: $H_0=100 \text{ km s}^{-1} \text{ Mpc}^{-1}$ and $q_0=0.5$. Wherever in the text we refer to linear sizes we introduce h^{-1} . Whenever the redshift for a particular source described in this paper is not available, a default value $z = 1.25$ providing the maximum linear size for a given angular size ($1''$ corresponds then to $4.3h^{-1} \text{ kpc}$) and the adopted cosmological model is assumed.

interstellar medium (ISM) is a basis of the so-called “frustration scenario”. According to this model, the small size of CSS sources may be attributed to the presence of dense clouds of ISM (van Breugel et al., 1984). However, to date there is no proof that such clouds are dense *enough* to impede further growth of the sources, so it is very plausible that the internal pressure of a CSS source is sufficient to allow expansion in ram pressure balance with the ambient ISM. Moreover, the infrared properties of GHz-Peaked Spectrum (GPS) and CSS sources are consistent with those of large-scale radio galaxies (Fanti et al., 2000). Hence, the existence of a dense medium that enshrouds galaxies hosting CSS sources and hampers the “normal” growth of a radio source remains unproven.

The notion that CSS sources are not frustrated but instead young has been present in the literature since the publication of the papers by Phillips & Mutel (1982) and Carvalho (1985). Fanti et al. (1995) provided a comprehensive theoretical background of the “youth scenario” which has subsequently been supported observationally. In particular, Murgia et al. (1999) showed that the spectral ages of CSS sources can be up to 10^5 years. Consequently, the youth scenario currently prevails over the frustration scenario; see the review by Fanti (2000). Support for this view has been brought by Siemiginowska et al. (2005) who observed diffuse X-ray emission around 3C186, a CSS identified with a QSO, using the *Chandra* X-ray Observatory. The discovery of a distant ($z = 1.063$) cluster associated with this CSS source provides direct observational evidence that at least this CSS source is not thermally confined, as required by the frustration scenario. Instead, it appears that 3C186 may be young and is observed at an early stage of its evolution.

If a CSS source lies close to the sky plane, it is perceived as a Medium-sized Symmetric Object (MSO), which is a scaled-down version of an FR II. Given that CSS sources are thought to be young, this similarity can be explained by an evolutionary scenario. Indeed, it has been argued (Readhead et al., 1996) that Compact Symmetric Objects (CSOs), MSOs and Large Symmetric Objects (LSOs) make up an evolutionary sequence. Double-lobed radio sources continually increase their size with time and LSOs begin their active phase as very compact sources and must have passed the CSO and MSO phases. However, the converse may not be true: it is not obvious that every CSO must become an LSO.

It also appears that there is no compelling reason to confine the CSS class only to the most powerful objects fulfilling the compactness and spectrum steepness criteria. In other words, the high radio power, typical for bright CSS sources, is not an essential ingredient of the definition of the CSS class. Indeed, the existence of weak CSS sources has been confirmed observationally; see Sect. 2. Three questions relating to these sources arise:

1. Are there any fundamental morphological differences between strong and weak CSS sources analogous to e.g. the well-known FRI/FRII division for LSOs which is clearly correlated with the radio luminosity (Fanaroff & Riley, 1974)?
2. Do weak CSS sources fit into the CSO–MSO–LSO evolutionary scheme developed by Readhead et al. (1996)?

3. What are the actual causes of the low power output?

This paper, along with its companion papers of the series, attempts to address the above questions based on new, high resolution observations of weak CSS sources selected from the *Faint Images of Radio Sky at Twenty* (FIRST) survey (White et al., 1997)². It is organised as follows. In Sect. 2 the selection procedure of the sample is presented. The technical details of the VLBI observations are given in Sect. 3 and the results of these observations supplemented with the earlier results of MERLIN survey are discussed in Sect. 4. Their astrophysical implications are discussed in Sect. 5 and summarised in Sect. 6.

2. The FIRST-based CSS sources sample

A number of samples of CSS sources other than 3CRPW have been generated so far. In particular, Fanti et al. (2001) derived a sample of 87 CSS sources from the B3-VLA sample (Vigotti et al., 1989) and the parsec-scale structures of many of them were studied using VLBI. Depending on the degree of the compactness of the sources they were followed up either with the EVN combined with MERLIN at 1.7 GHz (Dallacasa et al., 2002b) – hereafter D02b – or with the VLBA at three frequencies: 1.7 GHz (Dallacasa et al., 2002a) – hereafter D02a – and 5/8.4 GHz (Orienti et al., 2004).

The present study is based on a sample consisting of 60 sources extracted from FIRST. The details of the adopted selection procedure have been given in Kunert et al. (2002) – hereafter Paper I. Our selection criteria and those used by Fanti et al. (2001) were different, as were the RA and Dec limits of both samples, although the two samples are slightly overlapping. Therefore, a few sources described in this paper also belong to the B3-VLA CSS sample and so their independent VLBI observations have been reported in D02a, D02b and Orienti et al. (2004). Unlike the sources in the B3-VLA CSS sample, the ones dealt with here have steep spectra in a broad range of frequencies: $0.365 \leq \nu \leq 5$ GHz. This means that the GPS sources, which are sometimes treated as a separate subclass of the CSS class, have been deliberately excluded.

The sample was surveyed with MERLIN at 5 GHz by means of snapshot observations (a “pilot” survey) carried out in two sessions in 1997 and 1999; see Paper I for the technical details of those observations. Based on the angular sizes of radio structures detected by MERLIN, the whole sample was then divided into three groups. The first one consists of 11 objects with angular sizes in the range: $\sim 1'' - 5''$. Five of them were presented in Paper I. With one exception (1201+394) they have asymmetric structures. The remaining six objects are double or triple MSOs and were presented in Kunert-Bajraszewska et al. (2005) – hereafter Paper II.

The second group – hereafter Subsample Two – consists of 19 sources with angular sizes in the range $\sim 0.2 - 1''$ and the present paper (Paper III) is devoted to them. The basic parameters of their radio emission extracted from Texas (Douglas et al., 1996), FIRST and GB6 (Becker et al., 1991)

² Website: <http://sundog.stsci.edu>

Table 1. FIRST coordinates, flux densities and spectral indices of the sources in Subsample Two.

Source name (1)	RA (J2000) (2)	Dec (3)	$F_{365\text{MHz}}$ (4)	$F_{1.4\text{GHz}}$ [Jy] (5)	$F_{4.85\text{GHz}}$ (6)	$\alpha_{365\text{MHz}}^{1.4\text{GHz}}$ (7)	$\alpha_{1.4\text{GHz}}^{4.85\text{GHz}}$ (8)	$F_{1.655\text{GHz}}$ [Jy] (9)
0744+291*	07 48 05.332	29 03 22.54	1.25	0.48	0.17	-0.71	-0.83	0.41
0747+314	07 50 12.318	31 19 47.52	2.62	1.05	0.35	-0.68	-0.89	0.90
0811+360	08 14 49.068	35 53 49.70	1.71	0.58	0.17	-0.80	-0.99	0.49
0853+291	08 56 01.169	28 58 35.06	2.28	0.63	0.19	-0.95	-0.97	0.54
0902+416	09 05 22.197	41 28 39.65	1.10	0.48	0.17	-0.61	-0.86	0.42
0922+322*	09 25 32.727	31 59 52.87	1.80	0.53	0.20	-0.91	-0.79	0.47
1123+340	11 26 23.674	33 45 26.64	3.80	1.32	0.38	-0.79	-1.01	1.11
1232+295	12 34 54.387	29 17 43.79	1.10	0.46	0.16	-0.65	-0.84	0.40
1242+364	12 44 49.679	36 09 25.53	2.75	0.78	0.21	-0.94	-1.07	0.65
1251+308	12 53 25.750	30 36 35.03	1.03	0.45	0.20	-0.61	-0.66	0.41
1343+386	13 45 36.948	38 23 12.62	1.81	0.85	0.44	-0.56	-0.53	0.78
1401+353*	14 03 19.238	35 08 11.88	2.27	0.63	0.18	-0.96	-1.01	0.53
1441+409	14 42 59.307	40 44 28.79	1.51	0.97	0.30	-0.33	-0.94	0.83
1601+382*	16 03 35.150	38 06 42.93	0.99	0.43	0.20	-0.62	-0.61	0.39
1619+378	16 21 11.290	37 46 04.94	1.62	0.64	0.20	-0.69	-0.94	0.55
1632+391	16 34 02.910	39 00 00.18	1.98	0.93	0.37	-0.56	-0.74	0.82
1656+391	16 58 22.172	39 06 25.55	1.34	0.65	0.24	-0.53	-0.80	0.57
1709+303	17 11 19.939	30 19 17.67	1.83	1.03	0.37	-0.43	-0.83	0.90
1717+315	17 19 30.062	31 28 48.12	1.06	0.45	0.15	-0.63	-0.87	0.39

* Sources with names marked with an asterisk were not followed-up using VLBI.

Description of the columns: Col. (1): Source name in the IAU format; Col. (2): Source right ascension (J2000) extracted from FIRST; Col. (3): Source declination (J2000) extracted from FIRST; Col. (4): Total flux density at 365 MHz extracted from Texas Catalogue; Col. (5): Total flux density at 1.4 GHz extracted from FIRST; Col. (6): Total flux density at 4.85 GHz extracted from GB6; Col. (7): Spectral index ($S \propto \nu^\alpha$) between 365 and 1400 MHz calculated using flux densities in cols. (4) and (5); Col. (8): Spectral index between 1.4 and 4.85 GHz calculated using flux densities in cols. (5) and (6); Col. (9): Estimated total flux density at 1.655 GHz interpolated from data in cols. (5) and (6).

catalogues are listed in Table 1 and the redshifts, if available, and photometric data are given in Table 2. The magnitudes shown in cols. 5 and 6 are extracted from the POSS plates using the Automatic Plate Measuring (APM) machine whereas those in cols. 7 to 11 are taken from the Release 4 of the Sloan Digital Sky Survey (SDSS/DR4) which is the up-to-date version at the time of writing.

Objects in the third group – they are labelled ultra-compact steep spectrum objects – have angular sizes below $\sim 0''.2$ and were barely resolved with MERLIN at 5 GHz (resolution ≤ 50 milliarcseconds) in the course of the pilot survey. We found 16 such sources. Their milliarcsecond scale structures have been investigated by means of multifrequency VLBA observations and the results of that study are presented in Paper IV (Kunert-Bajraszewska et al., 2006) and Paper V (Kunert-Bajraszewska in prep.).

3. MERLIN and VLBI observations

MERLIN images of all 19 objects of Subsample Two are shown in Figs. 4 to 22 and they are discussed in Sect. 4. The maps are plotted to scale: their sizes are $3''.2 \times 3''.2$. Contours increase by a factor of 2 and the first contour is at $\sim 3\sigma$ level. Table 5 gives the flux densities of the main components of the structures derived from these images using AIPS task JMFIT.

Four sources (0744+314, 0922+322, 1401+353 and 1601+382) were not followed up using the VLBI technique as the MERLIN images did not show noticeable compact struc-

tures that would still be visible at milliarcsecond resolution. For the remaining 15 targets, two-frequency VLBI observations were carried out and their results are shown in Figs. 5 to 22 except Figs. 9, 15 and 17. As in the case of MERLIN maps, contours increase by a factor of 2 and the first contour is at $\sim 3\sigma$ level.

VLBI follow-up observations were carried out at two frequencies: 1.7 GHz with the VLBA and 5 GHz with the EVN. The angular resolutions of the two instruments are comparable at the quoted frequencies with typical beam sizes of $\approx 5 \times 8$ milliarcseconds (VLBA) and $\approx 7 \times 8$ milliarcseconds (EVN).

The VLBA observations were made in snapshot mode at 1655.4 MHz with 128 Mb/s recording (i.e. 2×32 MHz bandwidth) during three observing sessions as shown in Table 3. Each source was observed for 30–40 min in several scans of a typical length of 5 min. The data were correlated with the NRAO processor at Socorro. After system temperature calibration and antenna gain and correlator corrections had been applied, the data were further processed using standard AIPS procedures. The positions of target sources were established from interleaved observations of phase-reference sources. The locations of the maps' centres were then formally shifted to the strongest features using AIPS task UVFIX. (This procedure does not change the absolute positions of the target sources.)

The noise levels in the images resulting from the above observations are typically of $\sim 30 \mu\text{Jy}/\text{beam}$. A typical $u-v$ coverage achieved (for 1123+340) is shown in Fig. 1.

Table 2. Redshifts and photometric data of the sources in Subsample Two.

Source name (1)	z (2)	Ref. (3)	Opt. ID (4)	APM		SDSS/DR4				
				R (5)	B (6)	u (7)	g (8)	r (9)	i (10)	z (11)
0744+291			q	19.70	19.79	21.04	20.91	20.98	20.64	20.14
0747+314			G			22.55	23.55	20.87	19.02	19.24
0811+360			EF							
0853+291	1.085	(5)	Q	18.45	18.79	18.99	18.91	18.67	18.69	18.79
0902+416			G			22.55	22.67	21.77	21.07	20.27
0922+322			G			23.55	22.71	22.32	22.08	21.70
1123+340	1.247	(1)	G							
1242+364			G			23.87	21.94	21.57	21.23	20.30
1251+308			–	19.67	21.14					
1343+386	1.844	(2)	Q	17.69	–	18.42	18.24	18.05	17.60	17.52
1401+353	0.45 [†]	(3)	q	19.40	20.32	21.09	20.35	19.86	19.54	19.02
1441+409			EF							
1601+382			G	18.45	20.96	21.42	19.60	18.23	17.66	17.24
1619+378	1.271	(4)	Q	18.89	21.29	21.29	19.90	18.81	18.29	18.00
1632+391	1.085	(5)	Q	17.93	18.33	18.95	18.68	18.34	18.21	18.04
1656+391			G			24.08	22.04	20.26	19.56	19.13
1709+303			EF							

Description of the columns: Col. (1): Source name in the IAU format; Col. (2): Redshift; Col. (3): Reference for the redshift given in col. 2; Col. (4): Optical identification: G – galaxy, Q – QSO, EF – “empty field”, q – a star-like object with no known redshift; Cols. (5-6): Magnitudes for the two POSS/APM colours; Cols. (7-11): Magnitudes for the five SDSS colours.

[†]Photometric redshift.

References for redshifts: (1) – Rawlings et al. (2001), (2) – Hewitt & Burbidge (1989), (3) – Machalski (1998), (4) – Kock et al. (1996), (5) – SDSS.

Sources 1232+295 and 1717+315 are not listed since there is no data available for them to date and their possible optical counterparts are too faint to be measured using APM.

Note for optical identifications: “G” should be treated with caution as these designations mostly come from the “automated classifier” of SDSS.

The EVN snapshot observations were carried out in three observing sessions; see Table 3. In 1998 the array comprised the following telescopes: Cambridge, Effelsberg, Jodrell Bank Mk2, Medicina, Onsala (26 m), Toruń and Westerbork (tied array). Left-hand circular polarisation with a total bandwidth of 28 MHz (Mk IIIB standard) at 4961 MHz was recorded and the correlation was carried out using the Bonn correlator. In the second EVN session the telescopes were as listed above, but excluding Cambridge and including Noto. The observations were made at a frequency of 4971.5 MHz and with a bandwidth of 32 MHz. The two-bit sampled left-hand circular polarisation data were correlated at JIVE. Each source was observed for 30–40 min in several scans of a typical length of 5 min.

Calibration and further processing of the data were carried out using a standard procedure in AIPS. However, the absolute positions of the sources were established by using our 1.7-GHz VLBA images as initial models in the fringe-fitting algorithm (AIPS task FRING). Such a procedure does not change the absolute positions of the target sources more than a fraction of the beam size. The noise levels in the resulting images are typically $\sim 50 \mu\text{Jy}/\text{beam}$. The flux densities of the main components of the sources at the two frequencies derived using AIPS task JMFIT are given in Table 6.

A typical $u-v$ coverage during the EVN observations (for 1123+340) is shown in Fig. 2. The shortest VLBA spacings are a few times smaller than those available with the

EVN so that the sensitivity to the more extended elements of the images is much better in the case of the VLBA observations. Consequently, there is often an appreciable fraction of the “missing flux” in the EVN maps. In principle, this drawback could be removed by combining the EVN data with the MERLIN data from the pilot survey. Such data processing was attempted but it was unsuccessful mainly because of the snapshot mode of MERLIN observations.

Initial analysis of the observations of 1123+340 indicated that the source might be particularly interesting but the snapshot observations were insufficient for a definitive interpretation. Consequently, 1123+340 was re-observed in a dedicated EVN experiment at 5 GHz. The observation took place on 8 June 2001 with the participation of the Effelsberg, Jodrell Bank Mk2, Medicina, Noto, Onsala, Toruń and Westerbork telescopes. The resulting $u-v$ coverage is shown in Fig. 3. The observational configuration, the correlation and further data reduction were the same as for the EVN observations made on 11 Feb. 2001. Since the image of 1123+340 resulting from this observation is a considerable improvement upon that obtained from the observation of 16 Feb. 1998 – the noise level in the resulting image is $\sim 10 \mu\text{Jy}/\text{beam}$ – only the more recent image is included in this paper. Also, the data given for 1123+340 in Table 6 and discussion related to the EVN-based results for this source refer to the observation of 8 June 2001.

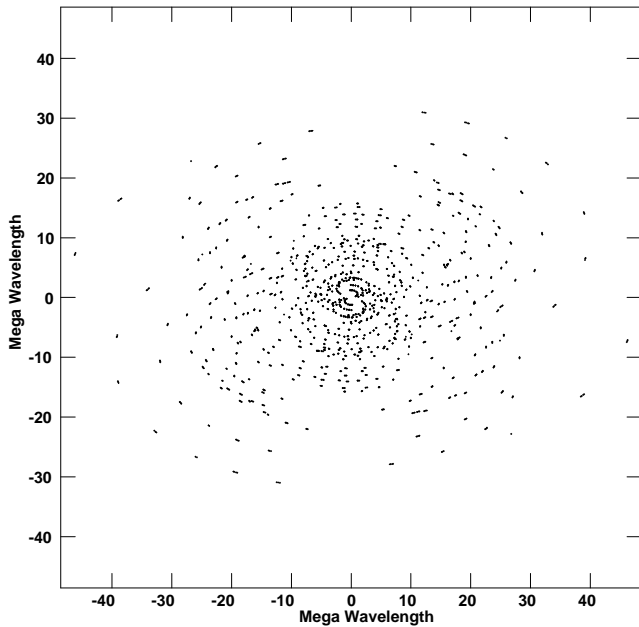


Fig. 1. Typical $u-v$ coverage during VLBA 1.7-GHz observations.

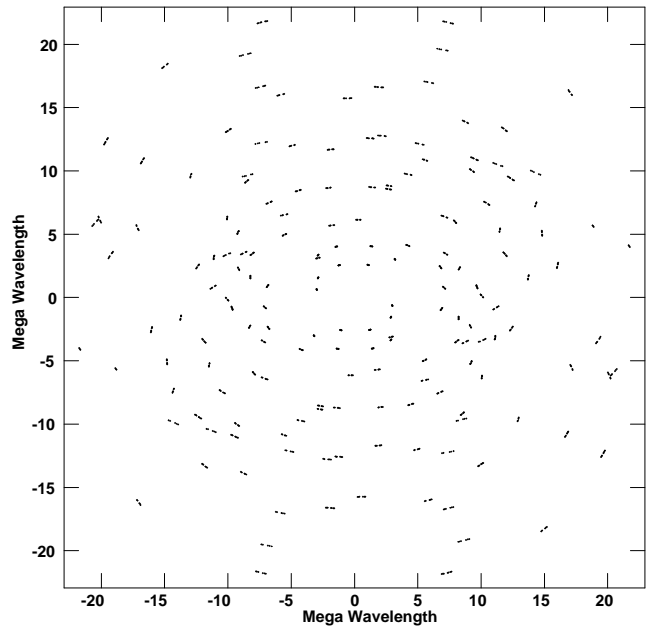


Fig. 2. Typical $u-v$ coverage during EVN 5-GHz observations.

Table 3. Journal and modes of VLBI observations.

Source	Networks, frequencies and recording systems		
	VLBA, 1.7 GHz	EVN, 5 GHz / recording	
0747+314	19 Sep 1998	16 Feb 1998	Mk IIIB
0811+360	"	"	
0902+416	"	"	
1123+340	"	"	
1232+295	"	"	
1242+364	"	"	
1251+308	"	"	
1619+378	30 Mar 2001	11 Feb 2001	Mk IV
1632+391	"	"	
1656+391	"	"	
1709+303	"	"	
1717+315	"	"	
0853+291	06 May 2001	11 Feb 2001	Mk IV
1343+386	"	"	
1441+409	"	"	
1123+340	—	8 Jun 2001	Mk IV

4. Notes on individual sources

The observational results for all 19 objects listed in Table 1 are commented on in this section. The morphological classification is summarised in Table 4.

0744+291 (Fig. 4). The northern component visible in the MERLIN 5-GHz image is very weak (2.4 mJy) so in principle this object consists of only one diffuse element. Only 47% of the GB6 flux density is present in the MERLIN image, indicating that there may exist an even more diffuse emission which is not reproduced there. The optical counterpart of this source – a $m_R = 20.98$ star-like object – is included in SDSS/DR4 although no redshift is available from there. It is located at

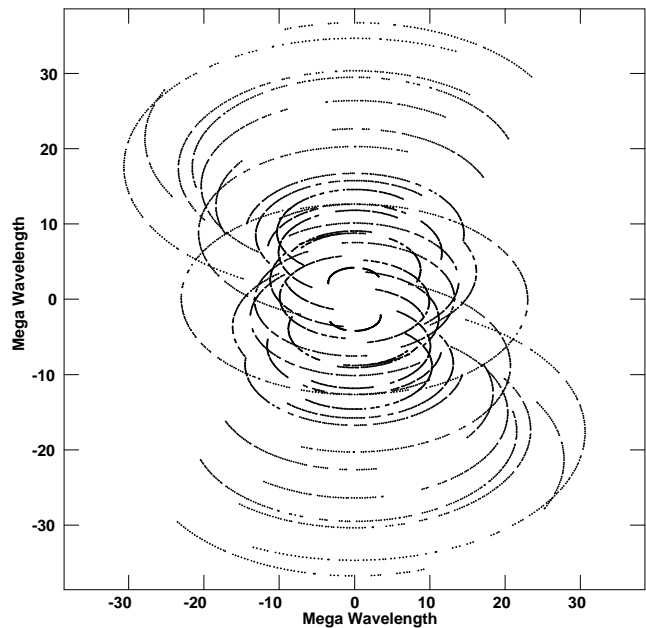


Fig. 3. The $u-v$ coverage during the 12-hour EVN observation of 1123+340 at 5 GHz.

RA= $7^{\text{h}}48^{\text{m}}05^{\text{s}}.229$, Dec= $+29^{\circ}03'23''.38$ i.e. $\sim 2''$ north-west of the position of the main radio feature. There is about 1-mag. difference between the APM and the SDSS measurements in both the red and the blue parts of the spectrum (Table 2) which may suggest variability.

This source can tentatively be interpreted as a relic lobe of an AGN located in the vicinity of this faint optical object and perhaps it ended its activity quite recently. The coordinates

Table 4. Morphological classification of the sources in Sample Two.

Type	Sources
Possible faders	0744+291, 0922+322, 1123+340†, 1656+391 (?)
Double-lobed	0747+314, 0811+360, 0902+416*, 1123+340‡, 1242+364, 1251+308 (?), 1441+409, 1656+391, 1709+303, 1717+315
Core-jet	1232+295, 1251+308 (?), 1343+386, 1601+382, 1619+378
Other	0853+291, 1401+353, 1632+391

*Classified as “double-lobed” based upon D02b.

†Applies to ‘E’ and ‘S’ components.

‡Applies to ‘N1/2’ and ‘W1/2’ components.

Some sources are listed more than once if they fulfill more than one criterion or if the classification is uncertain. Sources in the latter category are denoted with “?”.

of the main component in the MERLIN image coincide with those of the point-like object visible in the FIRST map. This means that there is no hint of the existence of the second lobe in FIRST, so even if such a lobe actually exists, it must be very faint. To make this interpretation viable it has to be assumed that the whole radio structure does not lie in the sky plane and that its observable part is more distant than the optical object which, in turn, is more distant than the putative second lobe. We can use the light-travel time argument, in a way similar to that in Owsianik et al. (1998), but substantially simplified; the “current activity period” – see their Fig. 3 – does not take place in the sources investigated here and we do not strictly require a restarted activity for them. It thus may be concluded that what is observed is the radio lobe of a switched-off AGN as seen in an epoch earlier than that of the optical object. An even later epoch emission from the other lobe is absent in the image either because the lobe has decayed completely or its spectrum has become very steep and so it is very weak at 5 GHz. There is another object in Subsample Two (0922+322) which could be interpreted in a similar manner – see below. In Sect. 5.3 the plausibility of the hypothesis used to interpret these two sources is discussed.

As the radio structure visible in the MERLIN image does not have a conspicuous compact component that might be an interesting target for follow-up observations at high resolution, 0744+291 was not imaged using VLBI.

0747+314 (Fig. 5). The 1.7-GHz milliarcsecond structure, particularly as seen in the VLBA image, leaves no doubt that the source is a classical, double-lobed triple with the central component being the core. A possible optical counterpart of this source is present in the SDSS/DR4 and identified with a $m_R = 20.87$ galaxy. A relatively bright ($\sim 13^m$) object (a field star?) is located $5''.78$ north of the position of the galaxy so only with SDSS is a correct optical identification possible. No redshift for that galaxy is available at the time of writing. The position

of the optical object (RA= $7^h50^m12^s342$, Dec= $+31^\circ19'47''.46$) does not coincide well with the position of the radio source (see Fig. 5) but given the diffuse shape of the optical object, the centroiding errors can be larger than usual and so it is a likely optical counterpart of the radio source.

The MERLIN image accounts for the entire GB6 flux density of this object. It was not possible to reproduce the core in the EVN image. Based on the value of the spectral index between 1.4 and 5 GHz and the flux densities at these frequencies, the interpolated total flux density of the source at 1.655 GHz (i.e. the VLBA observing frequency) has been calculated³ and listed in col. 9 of Table 1. It follows that the VLBA image accounts for 63% of the interpolated total flux density.

0811+360 (Fig. 6). This is a simple double source with both parts of roughly equal flux densities. The MERLIN image accounts for almost entire GB6 flux density of this object whereas the VLBA image accounts for 84% of the interpolated total flux density. No optical identification is available for this object in the literature. Based on the SDSS/DR4 image, which covers the field of 0811+360, this source has no optical identification.

0853+291 (Fig. 7). According to SDSS/DR4, the northeastern unresolved component seen in the MERLIN image is coincident with a QSO at a redshift of $z = 1.085$ located at RA= $8^h56^m01^s225$, Dec= $+28^\circ58'35''.50$ but it is the western part that is a dominating radio component. The 1.7-GHz VLBA image of that part, which accounts for only 10% of the interpolated total flux density, shows that there is a jet emerging from there towards east. To match it with the fuzzy structure seen in the MERLIN image it has to be assumed that the jet moves along a complicated, perhaps helical path. The 1.7-GHz VLBA image of the northeastern component identified with the optical object is also presented. It is slightly resolved and shows an extension oriented exactly towards the dominating component. The MERLIN image accounts for 76% of the GB6 flux density.

0902+416 (Fig. 8). This source belongs to the B3-VLA CSS sample and as such has been thoroughly investigated by D02b. The MERLIN image is fully consistent with the MERLIN 1.7-GHz image shown in D02b. The source has a double structure and almost entire GB6 flux density is accounted for in our image whereas there is a large discrepancy between our 1.7-GHz VLBA image and the EVN 1.7-GHz image presented in D02b; it was not possible to reproduce the northern lobe from the VLBA data. Our image accounts for only 47% of the interpolated total 1.7-GHz flux density.

This object is present in SDSS/DR4 and identified with a $m_R = 21.77$ galaxy. Its redshift is currently unknown. Its position (RA= $9^h05^m22^s189$, Dec= $+41^\circ28'39''.75$) is coincident with the brightest component in our VLBI images which is labelled “S2” in the D02b EVN image. This means that the “C” component in the D02b EVN image is less likely to be the core.

0922+322 (Fig. 9). According to SDSS/DR4, the northwestern unresolved component seen in the MERLIN image is coincident with a $m_R = 22.32$ galaxy of unknown redshift located at RA= $9^h25^m32^s674$, Dec= $+31^\circ59'52''.90$. The other component, because of its diffuse shape and a lack of a hotspot,

³ The same calculation has been carried out for the remaining sources in Subsample Two.

could be interpreted as a relic lobe somewhat similar to that in 0744+291. Only 38% of the GB6 flux density is accounted for in the MERLIN image. The northwestern component is a likely core and so the other lobe, which is unobservable at 5 GHz, should be located even farther north-west. It follows that a similar assumption as for 0744+291 could be made in this case, namely that the invisible northwestern lobe has completely dispersed. The combination of the source's possible linear size and the timescale of the dispersion make the light-travel delay an essential factor responsible for the apparent shape of this source. Further discussion and interpretation of 0922+322 is given in Sect. 5.3.

0922+322 is a member of 7C and 9C surveys (Waldram et al., 1996, 2003) and its 151-MHz and 15-GHz flux densities are 3410 and 68 mJy, respectively. It follows from these values supplemented with the measurements at three intermediate frequencies quoted in Table 1 that the source has had a steep spectrum throughout two decades of frequency.

0922+322 was not imaged using VLBI.

1123+340 (Fig. 10). In the 15-GHz VLA map this object appears as a compact double source (Naundorf et al., 1992). The MERLIN image confirms that apart from the two equally bright components a weaker one east of these two is also seen. (However, the restoring beam of the 15-GHz map by Naundorf et al. is five times larger so the eastern protrusion might not be resolved.) The MERLIN image accounts for 90% of the GB6 flux density so it seems to be fairly complete. The 1.7-GHz VLBA image that accounts for 75% of the interpolated total flux density at 1.7 GHz shows a very complicated structure.

The suggested interpretation is as follows. The field of 1123+340 encompasses *two* separate radio sources. One of them consists of the components labelled “E” and “S”. Based on the morphology alone, the “E” component resembles a lobe that is not edge brightened whereas the “S” component appears in the VLBA image as a collection of more than ten faint, compact subcomponents located in the area $\sim 50 \times 50$ milliarcseconds. We regard them as remnants of a lobe being at an advanced stage of decay. The “S” component does not appear in any of the 5-GHz images so that an assessment of its spectral index is impossible but it is obvious that the spectrum must be very steep.

It appears, therefore, that the components “E” and “S” are the lobes of a double source which is “dying”: there is no core or jet visible and the lobes are in the coasting phase. The projected linear size of this source is $1.9h^{-1}$ kpc. Assuming that the source does not lie exactly in the sky plane but the “S” lobe is closer to the observer, a simple interpretation of the difference between “E” and “S” is that “S” is seen at a later epoch, i.e. at a more advanced stage of the ageing process, and thus is more diffuse than “E”. The likely steepness of the spectrum of the “S” component explains why it is not visible at 5 GHz or at 15 GHz. The remaining components make a double source, “N2” being the putative core given it has the flattest spectrum.

Although this source is reminiscent of a lens such a possibility is unlikely (Browne, Rawlings priv. comm.).

The properties of 1123+340 will be further discussed in Sect. 5.2.

1232+295 (Fig. 11). The MERLIN image accounts for entire GB6 flux density. Its brightest central component most likely harbours the core and so the source has a triple structure. The 1.7-GHz VLBA image that accounts for 46% of the interpolated total flux density at 1.7 GHz shows quite a complicated core-jet structure. The core is the only component reproduced in the EVN image.

The most unusual feature of this source is that according to NVSS its fractional polarisation is 9.4%. Given that such high polarisation is not normally observed in CSS sources, particularly at low frequencies, 1232+295 may be intrinsically larger than normally attributed to CSS sources and substantial parts of its radio structure may lie outside of the inner 2-3 kpc region responsible for Faraday depolarisation (Fanti et al., 2004). Thus, this source may predominantly be distorted by beaming effects.

No optical counterpart of this object is known to date.

1242+364 (Fig. 12). In all the images shown, the source has a classic triple design with a core and two lobes. Component “C” in the VLBI images is most likely the core given that it is coincident with a $m_R = 21.57$ galaxy located at RA= $12^{\text{h}}44^{\text{m}}49^{\text{s}}.679$, Dec= $+36^{\circ}09'25''.50$ (The identification usually given in the literature – a ~ 20 mag. object – is in fact $6''.5$ off the position of the radio source towards the north-east.) It follows that the three compact components located between the core and the northern lobe are parts of a jet. The possibility that the source might be a gravitational lens system has been ruled out by King et al. (1999). The MERLIN image accounts for almost entire GB6 flux density of this object whereas the VLBA image accounts for 60% of the interpolated total flux density at 1.7 GHz. The spectrum of this source is one of the steepest among the sources in Subsample Two: $\alpha \approx -1.0$. The measurement at 10 GHz by Machalski & Inoue (1990) confirms this. At 151 MHz the source is slightly variable (Minns & Riley, 2000), however even assuming the maximum value of the flux density measured by Minns & Riley, the spectrum flattens below 365 MHz ($\alpha = -0.42$).

1251+308 (Fig. 13). The MERLIN image, which accounts for 66% of the GB6 flux density, suggests it might be a double source and the bright components at its extremities are connected by a bridge. This picture is roughly confirmed by the VLBA 1.7-GHz image but the extended low surface brightness “bridge” is poorly reproduced because of the lack of short spacings in the $u-v$ coverage. This is also indicated by the fact that the VLBA image accounts for only 30% of the interpolated total flux density at 1.7 GHz. Given that, at present, there is no known optical counterpart of this source, it is not possible to make a reliable classification – it can be either a simple core-jet (the northern feature being the core) or a double source.

1343+386 (Fig. 14). In the FIRST image there are two sources in this field: the one which is referred to in Table 1 and a 19 times weaker companion source $12''.8$ to the north. Whether the northern weak companion is related to the main one is unclear. The 1.46-GHz VLA map of 1343+386 by Machalski & Condon (1983) also shows that the brighter one seems to be a compact double. The MERLIN and EVN images confirm this but the 1.7-GHz VLBA image shows much more detail of the emission coming from the area between to two strongest components and fully confirms the image shown by

D02a. The VLBA image accounts for 83% of the interpolated total flux density at 1.7 GHz. Similarly, the MERLIN image accounts for 79% of the GB6 flux density. Having made a provision for a missing part of the 1.7-GHz flux and comparing it with MERLIN 5-GHz flux density we conclude that the component “N” (D02a denote it as “N1”) has a flat spectrum and so the source as a whole is of the core-jet type. The same conclusion has been reached by Orienti et al. (2004).

The optical identification of the source is a QSO at the redshift $z = 1.844$ located at RA=13^h45^m36^s.942, Dec=+38°23′12″.51. Given that CSOs are usually identified with galaxies but not quasars, this fact provides an additional constraint that 1343+386 is not a CSO.

1401+353 (Fig. 15). The 1.46-GHz VLA map presented by Machalski & Condon (1983) features a bright peak and a 5″ extension to the north-east. 1401+353 is present in SDSS/DR4 and identified with a $m_R = 19.86$ star-like object located at RA=14^h03^m19^s.309, Dec=+35°08′13″.28 so that it is coincident with the northeastern compact component seen in our MERLIN image. Thus, 1401+353 is an asymmetric triple where the northeastern extension visible in the Machalski & Condon (1983) map is a lobe while our MERLIN map shows the core and the other lobe. The MERLIN image accounts for all the GB6 flux density so that the northeastern lobe must have a steep spectrum.

According to NVSS, the fractional polarisation of 1401+353 is 5.3% which is unusual for CSS sources. To explain this it has to be assumed that, similarly to 1232+295, 1401+353 lies predominantly outside the inner region responsible for Faraday depolarisation. It follows that its intrinsic size must be larger than that of *bona fide* CSS sources and it is beamed to the observer so that it is foreshortened by the projection. A further consequence of such an assumption is that it is most likely a switched-off source and because of that, a core-jet structure, which is typical for beamed RLAGNs, is not observed here. The light-travel scenario works particularly well for such an orientation and so the conspicuous asymmetry of the whole object, as seen in the map by Machalski & Condon (1983), is explained.

1401+353 was not imaged using VLBI.

1441+409 (Fig. 16). The MERLIN image accounts for the entire GB6 flux density and it shows a simple core-jet structure whereas at least four components are present in the VLBI images. All of them have very steep spectra calculated based on the flux densities extracted from 1.7-GHz VLBA and 5-GHz EVN images. This is in an agreement with the fact that the source as a whole has a very steep spectrum between 1.4 GHz and 5 GHz ($\alpha = -0.94$) but between 365 MHz and 1.4 GHz the spectrum is relatively flat ($\alpha = -0.33$). In general, the source has a CSO layout. However, based on the VLBA and EVN images it is not possible to localize the core. 1441+409 belongs to the B3-VLA sample and its VLBA images are shown in D02a and Orienti et al. (2004). Only the 5-GHz VLBA image shown by Orienti et al. (2004) has a sufficient resolution and overall quality to pinpoint the core. Based on the SDSS/DR4 image, which covers the field of 1441+409, this source has no optical identification.

The VLBA image accounts for 84% of the interpolated total flux density at 1.7 GHz.

1601+382 (Fig. 17). This object is listed as a $m_R = 18.23$ galaxy in SDSS/DR4 and its optical position (RA=16^h03^m35^s.171, Dec=+38°06′42″.92) coincides with the strongest radio feature. It can be tentatively assumed that this is a core-jet source but spectral index information is required to confirm this. The MERLIN image accounts for 66% of the GB6 flux density. No VLBI follow-up has been made for this object. No redshift is known at the time of writing.

1619+378 (Fig. 18). The MERLIN image accounts for almost entire GB6 flux density and is made up of two main components. They are also present in the VLBI images; however, a large fraction of the flux is missing there mainly because the VLBI arrays could not reproduce the low surface brightness “bridge” seen in the MERLIN image. In the 1.7-GHz VLBA image which accounts for 43% of the interpolated total flux density at 1.7 GHz both components have roughly equal flux densities whereas in the EVN 5-GHz image the northeastern one is much weaker. This means it either has a steep spectrum or, because of its diffuseness, it could not be reproduced with the EVN snapshot observation. This is a clear hint that the northeastern feature is a lobe and so the south-west compact feature could be identified as a core. Thus, 1619+378 is asymmetric and could be a core-jet-lobe source.

1619+378 has an optical identification (a QSO) and its optical position given by SDSS/DR4 (RA=16^h21^m11^s.276, Dec=+37°46′04″.92) coincides with the feature labelled here as a core. The redshift of 1619+378 is $z = 1.271$ (Kock et al., 1996) and SDSS confirms this.

1632+391 (Fig. 19). This a QSO at $z = 1.085$. It has been included in the SDSS/DR4 and its optical position is RA=16^h34^m02^s.954, Dec=+39°00′00″.56. The MERLIN image accounts for 82% of the GB6 flux density whereas the VLBI observations account only for a minute fraction of the full flux density: at 1.7 GHz it is only 8% of the interpolated total flux density at 1.7 GHz, whereas at 5 GHz is it extremely low so that it was impossible to produce a map at all. Therefore, the bulk of the low frequency flux must come from a diffuse parts of the structure. The two southern diffuse components seen in the 1.7-GHz VLBA image seem to support this conjecture.

1656+391 (Fig. 20). According to the SDSS/DR4, this is a $m_R = 20.26$ galaxy at the position RA=16^h58^m22^s.185, Dec=+39°06′25″.58. In the radio domain this object is clearly a double. The MERLIN image accounts only for 54% of the GB6 flux density. The most striking feature of this source is that according to the 1.7-GHz VLBA image – it accounts for 63% of the interpolated total flux density at 1.7 GHz – both putative lobes of the source are not edge brightened as is normally expected in FR II-like objects. Moreover, since they are diffuse and contain no compact features (hotspots), the source is very poorly visible in the 5-GHz EVN image. It appears that 1656+391 may be a relic of a switched-off object.

1709+303 (Fig. 21). This object is clearly an edge brightened double and as such can be safely classified as a standard MSO. The MERLIN image accounts only for 47% of the GB6 flux density whereas the VLBA image accounts for 55%

of the interpolated total flux density at 1.7 GHz. According to SDSS/DR4, there is a $m_R = 21.27$ galaxy $\sim 0'.4$ south-west of the radio structure. It is not likely to be related to the radio source.

1717+315 (Fig. 22). This double source seems to have hotspots at the lobes' extremities – see the MERLIN image – but the VLBI observations poorly reproduce this. In particular, the source remains undetected with the EVN at 5 GHz. Most of the flux is also missing in the 1.7-GHz VLBA image (it accounts only for 24% of the interpolated total flux density at 1.7 GHz) so it is likely that the lobes are much more diffuse than might be expected based on the MERLIN image alone, which, in turn, accounts only for 30% of the GB6 flux density. There is no known optical counterpart of this source.

5. Discussion

5.1. The intermittent activity scenario

Reynolds & Begelman (1997) – hereafter RB97 – proposed a model in which extragalactic radio sources with modest linear sizes can be intermittent on timescales of $\sim 10^4$ – 10^5 years. They assume that an initially small source undergoes 10^4 year long bursts that recur every 10^5 years. When the power supply cuts off, the cocoon/shocked-shell system enters a coasting phase which is still pressure driven. Because of the drop in the source pressure, the radio luminosity of the cocoon will fall rapidly once the “central engine” has turned off. However, the shocked matter continues to expand supersonically and keeps the basic source structure unchanged. It is to be noted that the radiative losses were not included in the model so all of the fading is due to expansion. This model predicts that there should be a considerable number of MSOs which are weaker than those known so far because of the power cut-off.

RB97 do not investigate whether such short outbursts re-occurring relatively often can actually take place in radio-loud AGNs and if so, what sort of physical mechanism drives them. As suggested by Begelman (1999), it is possible to combine the RB97 model with the mechanism of thermal-viscous instabilities in the accretion disks of AGNs presented by Siemiginowska et al. (1996) and Siemiginowska & Elvis (1997). That theory has been further developed by Hatziminaoglou et al. (2001) and Janiuk et al. (2004). Further discussion of possible explanation of intermittency in radio sources by means of this theory is presented in Sect. 5 of Paper II.

It has been shown in this paper (but also in Paper II) that switched-off sources can have arbitrary linear sizes. It follows that the activity in a radio-loud AGN *can* cease at early stages of its evolution. The existence of such objects was predicted by RB97 and they may be responsible for the overabundance of small-scale radio sources (Begelman, 1999). This “population problem” was first noticed by O’Dea & Baum (1997) who pointed out that for the sources with linear sizes below a few kpc their number is constant regardless of the size. This cannot be easily solved in the framework of the “youth scenario”.

Begelman (1996) developed a simple model of the evolution of a radio source which treats it as a bubble expanding into

a radially stratified medium. It is assumed that the external density is governed by the power law: $n \propto r^{-\beta}$ and the luminosity is proportional to:

$$l^{(-\beta+4)/12}, \quad (1)$$

where l is the source’s linear size. The assumption of β between 1.5 and 2.0 is usually made and it is reasonable for the interstellar medium in giant elliptical galaxies. The number of sources per octave of size selected from a flux density limited sample obeys:

$$N(l) \propto l^{(28-11\beta)/24}. \quad (2)$$

To make the model consistent with the relationship $N \propto l^{0.4}$ observed for larger sources (O’Dea & Baum, 1997), $\beta \approx 1.7$ is to be assumed. For smaller sources $N = \text{const.}$ and so the parameter β has to be increased considerably. O’Dea & Baum (1997) put $\beta = 2.6$ within the inner few kpc which is effectively a variant of the frustration scenario, and – as they admit – it is hard to understand within the paradigm of the King-type model of the ISM. Following Begelman (1999), we suggest that the evolution of small sources is not necessarily different, and there is no need to adopt extreme values for β . Instead, the intermittency which manifests itself as a “premature” cease of the activity in particular phases of the source evolution can well account for the excess of small-scale sources.

5.2. The case of 1123+340: a switched-off object in a cluster

At the time of writing, this object is not included in SDSS, but according to Rawlings (priv. comm.) the radio source 1123+340 is identified with a near-IR giant elliptical galaxy located at RA = $11^{\text{h}}26^{\text{m}}23^{\text{s}}.654$, Dec = $+33^{\circ}45'26''.99$. That galaxy is most likely the N1/2 component of the 1.7-GHz VLBA image. There is only one definite emission line in the spectrum of this object so its redshift $z = 1.247$ is not certain (Rawlings et al., 2001). The near-IR image shows an appreciable number of red objects close to that galaxy – see the figure in Eales et al. (1997) – but the spectra show no evidence of any second redshift system (Rawlings priv. comm.). It is plausible that the 1123+340 field encompasses a cluster of galaxies and the two independent, very compact radio sources seen in the VLBI images are hosted by two galaxies of the cluster. Circumstantial evidence for the existence of a cluster is provided by the fact that N1/2 and W1/2 components form a double source with Wide-Angle-Tailed morphology which is a good tracer of the existence of the surrounding cluster.

Murgia et al. (2004) reported the discovery of three “dying” radio galaxies (they are sometimes termed “faders”; see Paper II and references therein) located at the centre of an X-ray emitting cluster. They argue that the association of faders with clusters implies that the pressure of the dense intracluster medium, perhaps a cooling flow, prevents a quick dispersion of a relic radio lobe through adiabatic expansion. Since the source expansion is reduced or even stopped, the chance of detecting relic radio lobes is higher than without the presence of intracluster gas. As shown in Sect. 4, the eastern double source seen

in the 1.7-GHz image (Fig. 10) is fader-like. Hence, our result is similar to that of Murgia et al. (2004) except that the fader seen in 1123+340 field is two orders of magnitude more compact than those presented by Murgia et al.

5.3. The asymmetries caused by light-travel time effect

It has been suggested in Sect. 4 that a number of sources dealt with here are “dying”; see Table 4. The major problem with accepting the above scenario is that according to the notion well established for the LSOs (Komissarov & Gubanov, 1994) – hereafter KG94:

- faders should have ultra steep spectra which is not the case for any of these sources,
- the “coasting phase” of the lobes of a formerly radio-loud AGN may last up to 10^8 years which is three orders of magnitude more than the (spectral) ages of the CSS sources (Murgia et al., 1999).

However, while the findings of KG94 are valid for LSOs with the linear sizes of the order of 1 Mpc, an important difference between LSOs and MSOs exists, namely that the latter ones have overpressured hotspots and probably the whole sources are overpressured⁴ due to their subgalactic sizes. Thus, when the jets switch off, the radio structure will still expand and suffer dramatic adiabatic losses which are explicitly neglected by KG94 but are likely to be much more effective in dimming a compact source than radiative losses taken into account by KG94 (Leahy, priv. comm.). Consequently, the theory developed by KG94 predicting long decay timescales that take place in coasting LSOs is not applicable to relics of CSS sources. As the expansion losses dominate in subgalactic-scale faders and they could occur in a comparatively short period of time – 10^5 years (RB97) – the lobes would quickly take the typical form of a fader without their spectra showing signs of ageing for frequencies below 5 GHz. This issue was raised in Paper II for the case of 1542+323 but more recently Giroletti et al. (2005) provided compelling evidence that, indeed, an MSO can take the form of a fader whereas its spectrum is not steeper than typical for CSS sources. One of the low-power compact sources they present, 1855+37, clearly shows the features of a fader: low power of the core, the lack of visible jets and diffuse lobes without hotspots. However, the spectral index between 1.4 and 5 GHz estimated from their plot is only $\alpha \approx -0.8$.

If a double-lobed radio source does not lie close to the sky plane then a significant time lag between the apparent stages of the evolution of the two lobes that are no longer fuelled should be observed. However, for the LSOs, even with linear sizes ≥ 1 Mpc, the light-travel time, i.e. the time lag between the images of the lobes as the observer perceives them, is about two orders of magnitude less than the timescale of the relic lobes decay time as given by KG94 and so in practice it is not observable. Contrary to that, in a (sub)galactic-scale source with a linear size of a typical galaxy diameter i.e. $\approx 10^5$ light years, the time lag between the images of both lobes starts to play a

role. This is because the lobes’ decay time is of a similar order of magnitude (10^5 years, RB97) as the time lag which, albeit shorter than the source linear size expressed in the light-travel time due to inclination of the source axis with respect to the sky plane, still has an order of magnitude of $\sim 10^5$ years provided the inclination angle is not very small. As a result, differences in the luminosities and morphologies of the lobes might become conspicuous.

In the case of an appreciable alignment of the source’s axis with respect to the line of sight, polarisation asymmetry is also expected, given that the larger parts of the source would have already been out of the “Faraday fog” found in the vicinity of the centre of the host galaxy. Moreover, an assumption that the source is in a switched-off state is necessary here to explain the lack of dominating core-jet structure coincident with the optical counterpart of the radio source as expected for a switched-on source. 1401+353 is perhaps a good example of a switched-off source beamed towards the observer.

The issue of luminosity asymmetries in CSS sources was thoroughly investigated both observationally (Saikia et al., 2001, 2002) and theoretically (Jeyakumar et al., 2005). They noticed that MSOs in general exhibit much larger asymmetries than LSOs and that this could be attributed to asymmetries in the distribution of gas on the opposite sides of the nucleus of the radio source. While this explanation remains valid both for “normal” sources where energy is currently transported to the lobes and “dying” sources, we suggest that the time-lag scenario outlined above may also play an important role in the case of the latter class of the sources. High dynamic range observations of the sources like 0744+291 and 0922+322 leading to a possible discovery of “missing” lobes and estimation of the spectral indices of both lobes are necessary to confirm the validity of the interpretation of the asymmetries by means of the rapid decay of relic lobes in compact sources and time lags due to the source orientation. Additionally, this would provide firm proof that the timescales of the decay of relic lobes in compact sources are indeed short, in accordance with RB97.

Finally, while we argue above that compact sizes of sources make the asymmetry caused by light-travel time effect more likely than in the case of LSOs, asymmetries of this kind *are* observed in objects appreciably larger than CSS sources. In TXS 1602+324 (Machalski & Condon, 1983) the southern lobe is devoid of a hotspot whereas the northern one is clearly of FR II type. It may be speculated that at a later stage of the evolution the southern lobe of TXS 1602+324 could fade out and become almost completely invisible while the northern one would remain observable. If this scenario actually develops, TXS 1602+324 might transform into a source similar to PKS 1400–33 (Subrahmanyan et al., 2003) where, indeed, only one lobe is observed.

5.4. Where are young FR Is?

For LSOs there are two distinct morphological Fanaroff–Riley classes and the FRI objects are less luminous at 178 MHz (Fanaroff & Riley, 1974). Given that according to the evolutionary scenario, 3CRPW CSS sources evolve towards FR II

⁴ For example, Siemiginowska et al. (2005) provided direct evidence that 3C186 is, indeed, overpressured.

radio galaxies, it can be speculated that there might be a relationship between weak CSS sources and FR Is. In the simplest form such a relationship would mean a morphological similarity of a weak CSS source to an FRI. However, among the sources investigated here the FRI-like morphology is never observed. This not difficult to interpret taking into account that CSS sources have subgalactic linear sizes. The propagation in the atmosphere of the host galaxy will tend to keep the jets overpressured, and so to maintain sources as FR IIs until they exit the galaxy atmosphere (see e.g. Carvalho & O’Dea, 2002). This would suggest that a possible transition from “post-CSS” FR II phase to FRI would only occur once the radio source has propagated well beyond the host galaxy.

Orienti et al. (2004) claim they have found two FRI-like CSS sources in their sample – 1242+410 and 2358+406 – but in our opinion this interpretation is uncertain. 1242+410 is a QSO so the radio source is likely to be distorted by beaming and 2358+406, although it resembles an FRI in the 1.7-GHz image (D02a), has a quite complicated, multiple structure in 5 and 8.4-GHz images (Orienti et al., 2004).

Nevertheless, a relationship between weak CSS sources and FR Is might exist. According to the “bubble model” (Begelman, 1996), a ~ 100 pc-sized source after having evolved into 100 kpc source would decrease its luminosity by a factor of 20. This means that only bright CSS sources would evolve into FR IIs. Thus, it cannot be ruled out that weak CSS sources, even if they resemble FR IIs at the MSO stage, are progenitors of large-scale FR Is (Snellen et al., 2000). However, the transition from an FR II to FRI phase is still not well understood, although it has been predicted by Ghisellini & Celotti (2001).

6. Conclusions

The conclusions of the study of 19 weak CSS sources with sizes below $\approx 1''$ presented here are as follows.

1. The sources in Subsample Two have a variety of morphological types as shown in Table 4. Such a variety remains in agreement with the general picture drawn by Fanti et al. (1990) that CSS sources are intrinsically small and can be randomly oriented with regard to the sky plane. However, there are only 3 quasars among the objects investigated. Therefore, distortions caused by beaming perhaps play a secondary role compared to those resulting from the asymmetries in the distribution of host galaxy ISM (but see also point 3. below).
2. The well established youth scenario remains valid. However, an important factor has been added to it: the activity of AGNs hosting young radio sources can be intermittent and so they can “die early”. At least three sources with clear signs of ceased activity have been found. The relic object in 1123+340 field is of a particular importance. It is most likely a member of a cluster of galaxies and as such it is immersed in the intracluster gas which slows down the dispersion of the lobes and so helps to preserve their shape.
3. According to RB97, the timescale of the drop in the radio luminosity of “dying” CSS sources is of the order of 10^5 years. It could therefore be comparable to the light-travel time across the source itself. Unless the source does not lie in the sky plane, the apparent differences in the evolutionary stages of coasting lobes can be visible and take the form of high asymmetries in the images of its lobes which, intrinsically, can be quite symmetric.
4. None of the sources has an FRI morphology, which is in agreement with the notion that the FRI-like structures develop only above the atmosphere of the host galaxy. It is not excluded, however, that weak CSS sources *can* eventually become FR Is but the transition from FR II-type morphology typical for CSS sources to FRI-type morphology remains unclear.

Acknowledgements.

MERLIN is operated by the University of Manchester as a National Facility on behalf of the Particle Physics & Astronomy Research Council (PPARC).

The VLBA is operated by the National Radio Astronomy Observatory (NRAO), a facility of the National Science Foundation (NSF) operated under cooperative agreement by Associated Universities, Inc. (AUI). JIVE is the Joint Institute for Very Long Baseline Interferometry in Europe. It was created by the European Consortium for VLBI and is a member of the European VLBI Network (EVN). Its primary task is to operate the EVN Mk IV VLBI Data Processor.

The Automatic Plate Measuring (APM) machine is a National Astronomy Facility run by the Institute of Astronomy in Cambridge (UK). Official website: <http://www.ast.cam.ac.uk/~apmcat>.

Use has been made of the fourth release of the Sloan Digital Sky Survey (SDSS) Archive. Funding for the creation and distribution of the SDSS Archive has been provided by the Alfred P. Sloan Foundation, the Participating Institutions, the National Aeronautics and Space Administration, the National Science Foundation, the U.S. Department of Energy, the Japanese Monbukagakusho, and the Max Planck Society. The SDSS Web site is <http://www.sdss.org/>. The SDSS is managed by the Astrophysical Research Consortium (ARC) for the Participating Institutions. The Participating Institutions are The University of Chicago, Fermilab, the Institute for Advanced Study, the Japan Participation Group, The Johns Hopkins University, Los Alamos National Laboratory, the Max-Planck-Institute for Astronomy (MPIA), the Max-Planck-Institute for Astrophysics (MPA), New Mexico State University, University of Pittsburgh, Princeton University, the United States Naval Observatory, and the University of Washington.

This research has made use of the NASA/IPAC Extragalactic Database (NED) which is operated by the Jet Propulsion Laboratory, California Institute of Technology, under contract with the National Aeronautics and Space Administration.

Part of this research was made when MK-B stayed at Jodrell Bank Observatory and received a scholarship provided by the EU under the Marie Curie Training Site scheme.

Interesting discussions on thermal-viscous instabilities with Bożena Czerny and Agnieszka Janiuk made our findings on the role of that mechanism clearer.

We are very grateful to Peter Thomasson for suggestions leading to a significant improvement of this paper.

We thank the referee for a comprehensive report and discussion.

References

- Akujor, C. E., & Garrington, S. T. 1995, *A&AS*, 112, 235
 Becker, R. H., White, R. L., & Edwards, A. L. 1991, *ApJS*, 75,

- Begelman, M. C. 1996, in *Proceedings of the Greenbank Workshop, Cygnus A – A Study of a Radio Galaxy*, ed. C. L. Carilli, & D. E. Harris, CUP, Cambridge, p. 209
- Begelman, M. C. 1999, *The Most Distant Radio Galaxies*, *Proceedings of the colloquium, Amsterdam, 15-17 October 1997*, ed. H. J. A. Röttgering, P. N. Best, & M. D. Lehnert, Royal Netherlands Academy of Arts and Sciences, p. 173. [arXiv:astro-ph/9712107]
- van Breugel, W. J. M., Miley, G. K., & Heckman, T. A. 1984, *AJ*, 89, 5
- Carvalho, J. C. 1985, *MNRAS*, 215, 463
- Carvalho, J. C., & O’Dea, C. P. 2002, *ApJS*, 141, 371
- Dallacasa, D., Tinti, S., Fanti, C., et al. 2002a, *A&A*, 389, 115 (D02a)
- Dallacasa, D., Fanti, C., Giacintucci S., et al. 2002b, *A&A*, 389, 126 (D02b)
- Douglas, J. N., Bash, F. N., Arakel Bozayan, F., & Torrence, G. W. 1996, *AJ*, 111, 1945
- Eales, S., Rawlings, S., Law-Green, D., Cotter, G., & Lacy, M. 1997, *MNRAS*, 291, 593
- Fanaroff, B. L., & Riley, J. M. 1974, *MNRAS*, 167, 31P
- Fanti, R., Fanti, C., Schilizzi, R. T., et al. 1990, *A&A*, 231, 333
- Fanti, C., Fanti, R., Dallacasa, D., et al. 1995, *A&A*, 302, 317
- Fanti, C., Pozzi, F., Fanti, R., et al. 2000, *A&A*, 358, 499
- Fanti, C. 2000, *Proceedings of the 5th European VLBI Network Symposium held at Chalmers University of Technology, Gothenburg, Sweden, June 29 – July 1, 2000*, Eds.: J. E. Conway, A. G. Polatidis, R. S. Booth and Y. M. Pihlström, p. 73
- Fanti, C., Pozzi, F., Dallacasa, D., et al. 2001, *A&A*, 369, 380
- Fanti, C., Branchesi, M., Cotton, W. D., et al. 2004, *A&A*, 427, 465
- Ghisellini, G. & Celotti, A. 2001, *A&A*, 379, L1
- Giroletti, M., Giovannini, G. & Taylor, G. B. 2005, *A&A*, 441, 89
- Hatziminaoglou, E., Siemiginowska, A., & Elvis, M. 2001, *ApJ*, 547, 90
- Hewitt, A. & Burbidge, G. 1989, *magnetic tape*
- Janiuk, A., Czerny, B., Siemiginowska, A., & Szczerba, R. 2004, *ApJ*, 602, 595
- Jeyakumar, S., Wiita, P. J., Saikia, D. J., & Hooda, J. S. 2005, *A&A*, 432, 823
- King, L. J., Browne, I. W. A., Marlow, D. R., Patnaik, A. R., & Wilkinson, P. N. 1999, *MNRAS*, 307, 225
- Kock, A., Meisenheimer, K., Brinkmann, W., Neumann, M., & Siebert, J. 1996, *A&A*, 307, 745
- Komissarov, S. S. & Gubanov, A. G. 1994, *A&A*, 285, 27 (KG94)
- Kunert, M., Marecki, A., Spencer, R. E., Kus, A. J., & Niezgodna, J. 2002, *A&A*, 391, 37 (Paper I)
- Kunert-Bajraszewska, M., Marecki, A., Thomasson, P., & Spencer, R. E. 2005, *A&A*, 440, 93 (Paper II)
- Kunert-Bajraszewska, M., Marecki, A., & Thomasson, P. 2006, *A&A* (in press) (Paper IV) [arXiv:astro-ph/0601288]
- Lüdke, E., Garrington, S. T., Spencer, R. E., et al. 1998, *MNRAS*, 299, 467
- Machalski, J. & Condon, J. J. 1983, *AJ*, 88, 143
- Machalski, J. 1998, *A&AS*, 128, 153
- Machalski, J. & Inoue, M. 1990, *MNRAS*, 243, 209
- Minns, A. R. & Riley, J. M. 2000, *MNRAS*, 315, 839
- Murgia, M., Fanti, C., Fanti, R., et al. 1999, *A&A*, 345, 769
- Murgia, M., Parma, P., de Ruiter, H. R., Mack, K.-H., & Fanti, R. 2004, *X-Ray and Radio Connections – workshop on observations and theory in the X-ray and radio wavebands, Santa Fe (NM), 3-6 Feb. 2004* [arXiv:astro-ph/0405091]
- Naundorf, C. E., Alexander, P., Riley, J. M., et al. 1992, *MNRAS*, 258, 647
- O’Dea, C. P. & Baum, S. A. 1997, *AJ*, 113, 148
- O’Dea, C. P. 1998, *PASP*, 110, 493
- Orienti, M., Dallacasa, D., Fanti, C., et al. 2004, *A&A*, 426, 463
- Owsianik, I., Conway, J. E., & Polatidis, A. G. 1998, *A&A*, 336, L37
- Peacock, J. A. & Wall, J. V. 1982, *MNRAS*, 198, 843
- Phillips, R. B. & Mutel, R. L. 1982, *A&A*, 106, 21
- Rawlings, S., Eales, S., & Lacy, M. 2001, *MNRAS*, 322, 523
- Reynolds, C. S. & Begelman, M. C. 1997, *ApJ*, 487, L135 (RB97)
- Readhead, A. C. S., Taylor, G. B., Xu, W., et al. 1996, *ApJ*, 460, 612
- Saikia, D. J., Kodali, P. D., & Swarup, G. 1985, *MNRAS*, 216, 385
- Saikia, D. J., Singal, A. K., & Cornwell, T. J. 1987, *MNRAS*, 224, 379
- Saikia, D. J., Jeyakumar, S., Salter, C. J., et al. 2001, *MNRAS*, 321, 37
- Saikia, D. J.; Thomasson, P.; Spencer, R. E., et al. 2002, *A&A*, 391, 149
- Subrahmanyan, R., Beasley, A. J., Goss, W. M., Golap, K., & Hunstead, R. W. 2003, *AJ*, 125, 1095
- Siemiginowska, A. & Elvis, M. 1997, *ApJ*, 482, L9
- Siemiginowska, A., Czerny, B., & Kostyunin, V. 1996, *ApJ*, 458, 491
- Siemiginowska, A., Cheung, C. C., LaMassa, S., et al. 2005, *ApJ*, 632, 110
- Snellen, I. A. G., Schilizzi, R. T., Miley, G. K., et al. 2000, *MNRAS*, 319, 445
- Spencer, R. E., McDowell, J. C., Charlesworth, M., et al. 1989, *MNRAS*, 240, 657
- Vigotti, M., Grueff, G., & Perley, R. 1989, *AJ*, 98, 419
- Waldram, E. M., Yates, J. A., Riley, J. M., & Warner, P. J. 1996, *MNRAS*, 282, 779
- Waldram, E. M., Pooley, G. G., Grainge, K. J. B., et al. 2003, *MNRAS*, 342, 915
- White, R. L., Becker, R. H., Helfand, D. J., & Gregg, M. D. 1997, *ApJ*, 475, 479

Online Material

Table 5. Fitted parameters of the MERLIN map components.

Source name (1)	R.A. (2)	Dec (3)	$S_{5\text{GHz}}$ [mJy] (4)	θ_1 [mas] (5)	θ_2 [mas] (6)	P.A. [deg.] (7)	Opt. ID (8)
0744+291	07 48 05.314	29 03 22.72	2.4	121	95	114	
	07 48 05.335	29 03 22.25	77.5	124	80	107	
0747+314	07 50 12.311	31 19 47.57	166.6	36	23	74	
	07 50 12.316	31 19 47.58	72.0	19	14	84	
	07 50 12.330	31 19 47.60	163.7	32	17	73	
0811+360	08 14 49.066	35 53 49.72	71.4	22	6	114	
	08 14 49.077	35 53 49.67	81.9	14	7	130	
0853+291	08 56 01.153	28 58 34.81	20.4	292	65	171	
	08 56 01.161	28 58 34.87	72.9	299	91	36	
	08 56 01.164	28 58 35.12	44.7	83	43	167	
	08 56 01.226	28 58 35.48	5.6	0	0	—	•
0902+416	09 05 22.185	41 28 39.70	129.6	74	12	171	•
	09 05 22.190	41 28 39.96	19.6	47	39	174	
0922+322	09 25 32.679	31 59 52.98	2.1	0	0	—	•
	09 25 32.753	31 59 52.29	73.5	185	118	133	
1123+340	11 26 23.651	33 45 26.83	141.0	36	16	25	
	11 26 23.667	33 45 26.97	147.9	67	24	90	
	11 26 23.674	33 45 26.95	46.7	75	34	118	
1232+295	12 34 54.373	29 17 43.96	56.5	93	63	119	
	12 34 54.380	29 17 43.87	106.7	149	47	131	
	12 34 54.387	29 17 43.80	10.0	16	5	137	
	12 34 54.379	29 17 43.95	18.4	20	7	52	
1242+364	12 44 49.672	36 09 25.35	51.3	36	33	90	
	12 44 49.685	36 09 25.53	20.2	71	38	32	•
	12 44 49.700	36 09 25.77	115.0	63	17	53	
1251+308	12 53 25.736	30 36 35.28	36.0	17	6	113	
	12 53 25.741	30 36 35.18	4.5	26	12	167	
	12 53 25.745	30 36 34.99	17.3	88	78	123	
	12 53 25.747	30 36 34.91	15.2	76	47	3	
	12 53 25.750	30 36 34.74	57.8	35	14	146	
1343+386	13 45 36.949	38 23 12.59	88.5	25	13	167	
	13 45 36.951	38 23 12.49	260.9	17	12	135	
1401+353	14 03 19.231	35 08 11.81	36.9	81	53	8	
	14 03 19.240	35 08 11.70	57.4	31	0	150	
	14 03 19.244	35 08 11.97	73.0	151	61	39	
	14 03 19.319	35 08 13.34	3.5	35	18	83	•

Table 5. continued

Source name (1)	R.A. (2)	Dec (3)	S _{5GHz} [mJy] (4)	θ_1 [mas] (5)	θ_2 [mas] (6)	P.A. [deg.] (7)	Opt. ID (8)
1441+409	14 42 59.327	40 44 29.01	317.4	90	14	63	
1601+382	16 03 35.182	38 06 42.83	64.3	70	30	1	•
	16 03 35.185	38 06 43.06	37.1	222	98	41	
	16 03 35.187	38 06 43.04	10.1	153	37	121	
	16 03 35.190	38 06 43.28	21.4	86	32	175	
1619+378	16 21 11.278	37 46 04.69	5.7	69	63	30	•
	16 21 11.286	37 46 04.89	68.9	31	12	53	
	16 21 11.299	37 46 05.05	9.7	209	99	64	
	16 21 11.316	37 46 05.26	101.2	62	50	60	
1632+391	16 34 02.925	39 00 00.20	113.5	142	94	47	•
	16 34 02.940	39 00 00.29	122.4	114	74	25	
	16 34 02.952	39 00 00.38	57.7	55	53	32	
	16 34 02.963	39 00 00.63	13.5	34	22	164	
1656+391	16 58 22.176	39 06 25.63	90.1	21	12	112	
	16 58 22.185	39 06 25.56	42.1	24	13	115	
1709+303	17 11 19.930	30 19 17.92	71.0	46	34	164	•
	17 11 19.959	30 19 17.73	102.6	49	19	114	
1717+315	17 19 30.062	31 28 48.34	33.2	100	45	114	
	17 19 30.095	31 28 48.28	5.0	130	77	78	
	17 19 30.104	31 28 48.30	8.3	39	31	102	

In column (8) indication is given which component is uniquely identified with SDSS/DR4 optical object.

Table 6. Fitted parameters of the 1.7-GHz VLBA and 5-GHz EVN maps components.

Source name (1)	Component(s) (2)	$S_{1.7\text{GHz}}$ [mJy] (3)	θ_1 [mas] (4)	θ_2 [mas] (5)	P.A. [deg.] (6)	$S_{5\text{GHz}}$ [mJy] (7)	θ_1 [mas] (8)	θ_2 [mas] (9)	P.A. [deg.] (10)				
0747+314	E1	277.3	23	12	59	49.4	14	4	58				
	E2	9.2	18	6	105								
	C	8.0	11	–	–								
	W2	3.1	26	7	53								
	W1	274.6	19	15	46					39.8	10	6	46
0811+360	E	206.0	14	10	160	46.0	11	3	174				
	W	204.7	21	9	118	36.6	10	2	143				
0853+291	C	6.1	10	5	72	11.0	1	–	–				
	M	48.5	13	12	112								
	S	4.8	24	14	105								
0902+416	C	51.9	10	8	170	17.7	2	–	–				
	S	144.5	31	22	172	4.2	7	5	56				
1123+340	E	46.0	33	12	32	17.4	12	5	57				
	N1	90.7†	28	8	60								
	N2									11.1	12	5	56
	N3	111.4	8	5	75					50.8	3	2	92
	W1	388.1	14	13	92					60.3	11	8	113
	W2	164.6	15	12	43					20.0	13	3	76
	W3	9.4	7	1	112					5.9	9	4	109
1232+295	E1	11.2	26	10	116	1.6	4	3	107				
	E2	43.7	38	11	114								
	E3	37.1	28	9	112					10.3	12	–	–
	E4	29.0	26	10	130								
	E5	9.6	26	15	168								
	W1	11.2	35	11	42								
	W2	31.1	29	11	22								
1242+364	N2	247.5	26	13	108	11.3	14	2	113				
	N1	60.1	17	7	26	14.3	2	–	–				
	C	16.7	4	–	–								
	S	68.8	15	12	160					9.0	5	3	133
1251+308	N2	50.2	17	5	109	18.1	4	–	–				
	N1	6.1	23	12	141	18.1	4	–	–				
	S	64.6	33	20	143								
1343+386	N	69.0	8	4	178	46.5	2	1	14				
	C	15.1	12	6	164	136.7	4	4	46				
	S	559.1	9	7	121								
1441+409	E	119.6	12	9	26	12.2	5	1	145				
	C	165.7	15	3	71	46.1	15	2	70				
	W	405.5	11	7	64	95.7	6	4	54				
1619+378	L	120.7	23	19	168	5.5	7	4	85				
	C	118.5	20	3	55	41.4	10	1	58				
1632+391	C	12.1	7	–	–								
	M	26.0	15	12	162								
	W	28.3	25	22	38								
1656+391	E	96.2	22	13	121	15.6	18	10	91				
	W	265.5	22	16	121								
1709+303	E	324.6	31	19	136	18.1	7	2	169				
	W	165.9	20	10	128	31.5	5	3	117				
1717+315	E	19.5	26	13	48								
	W	75.1	31	20	93								

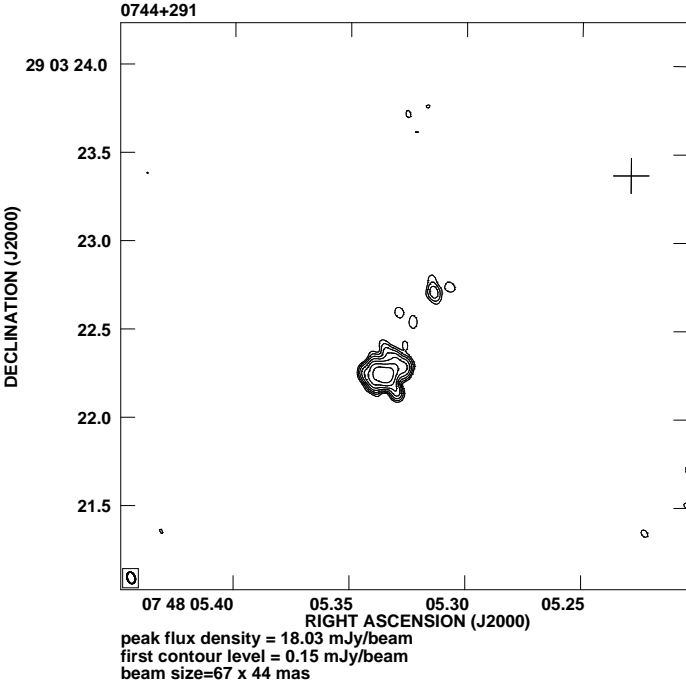


Fig. 4. MERLIN map of 0744+291 at 5 GHz. The cross indicates the position of an optical object in SDSS/DR4.

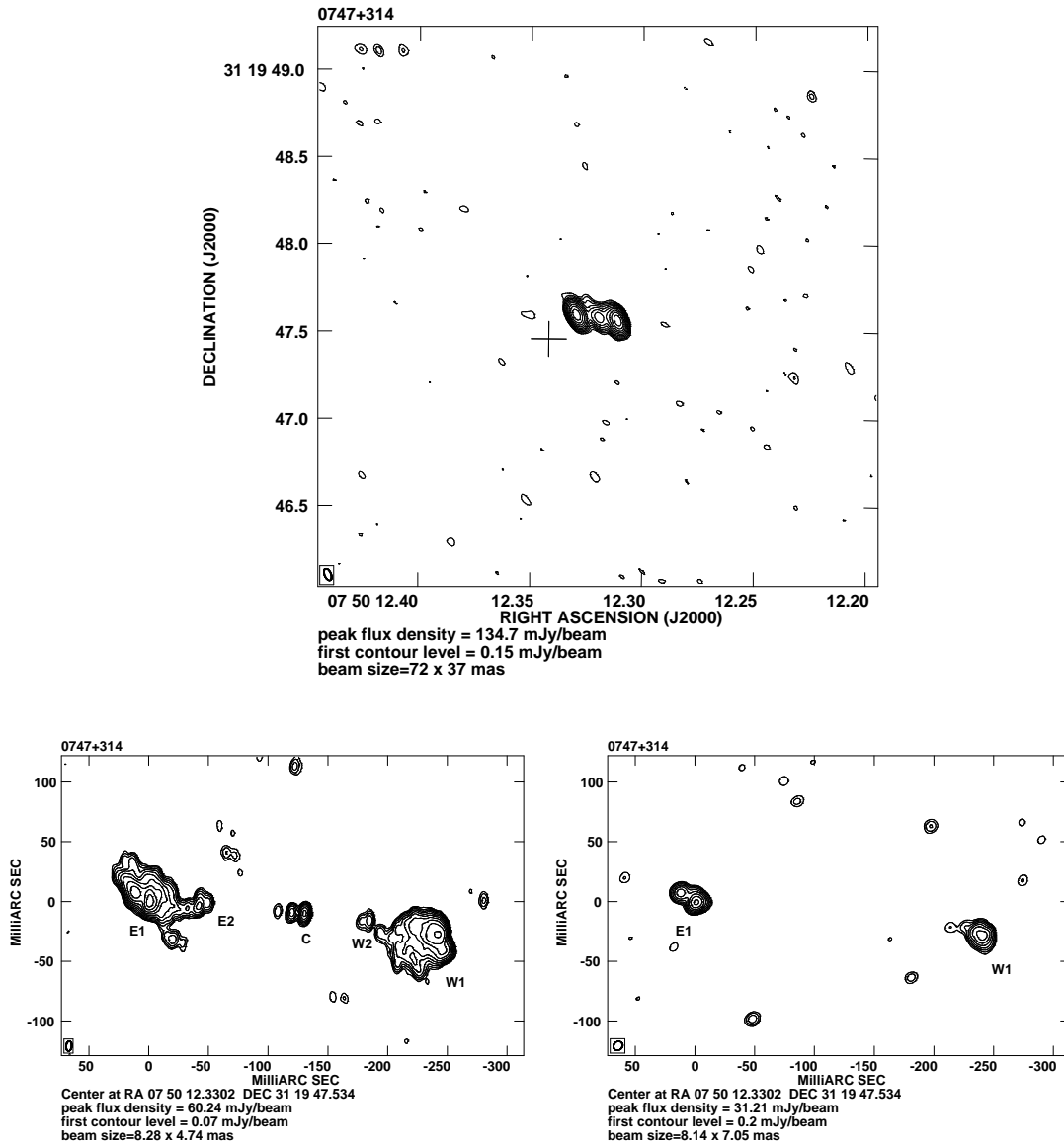


Fig. 5. 0747+314 — MERLIN map at 5 GHz (upper panel), VLBA map at 1.7 GHz (lower left panel) and EVN map at 5 GHz (lower right panel). The cross on the MERLIN map indicates the position of an optical object in SDSS/DR4.

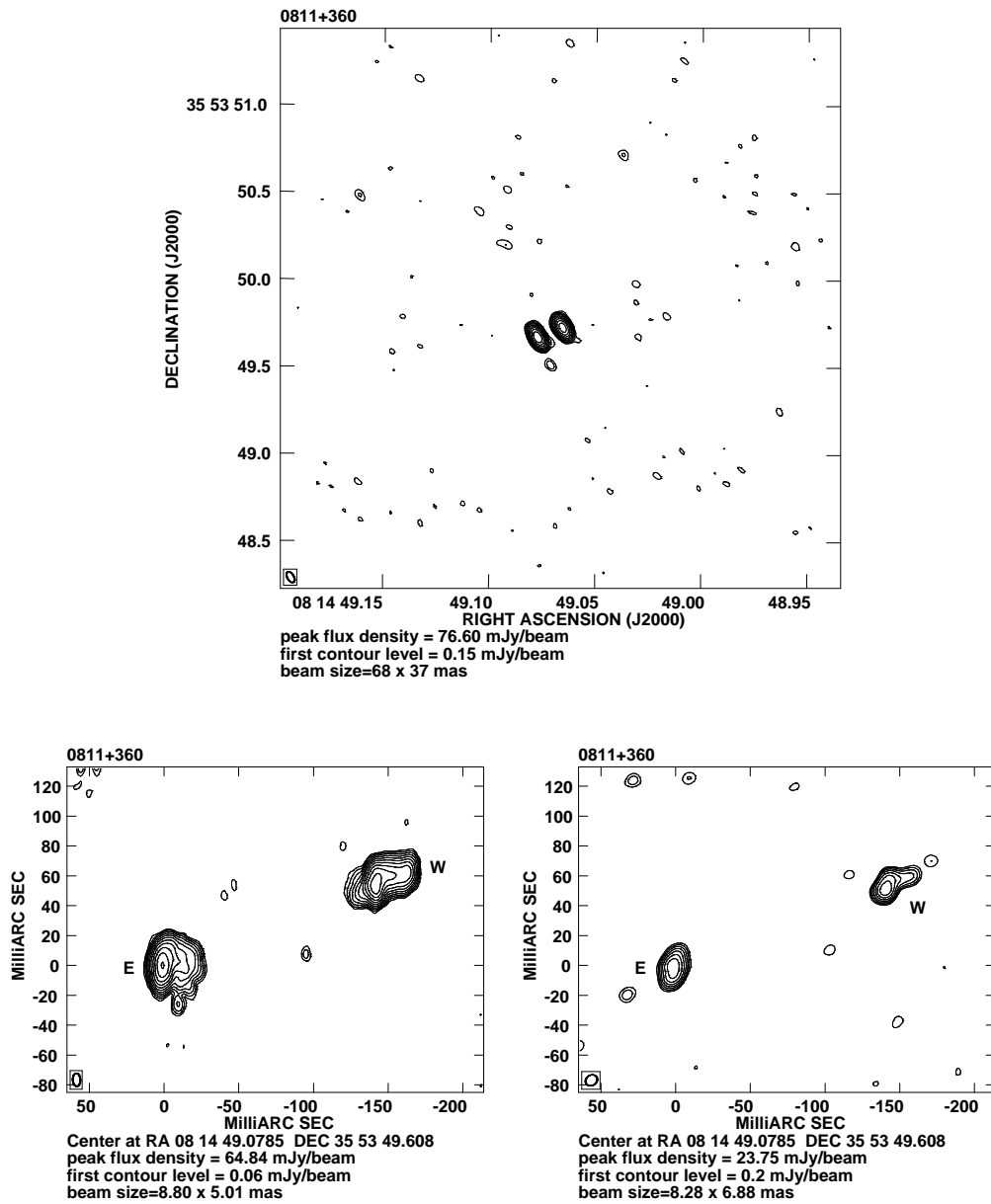


Fig. 6. 0811+360 — MERLIN map at 5 GHz (upper panel), VLBA map at 1.7 GHz (lower left panel) and EVN map at 5 GHz (lower right panel).

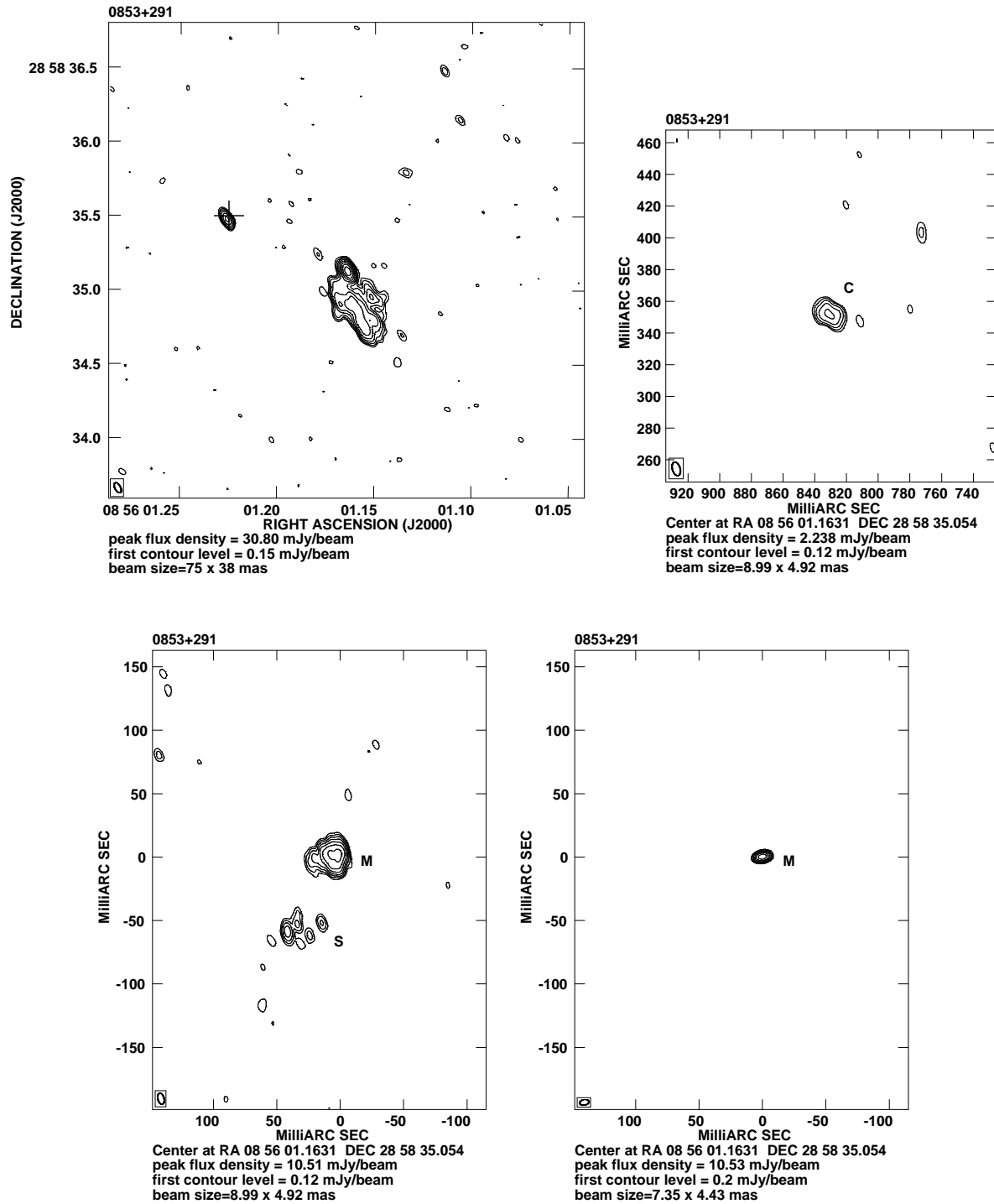


Fig. 7. 0853+291 — MERLIN map at 5 GHz (upper left panel), VLBA map at 1.7 GHz of the north-eastern component (upper right panel), VLBA map at 1.7 GHz (lower left panel) of the central component and EVN map at 5 GHz of the central component (lower right panel). The cross on the MERLIN map indicates the position of an optical object in SDSS/DR4.

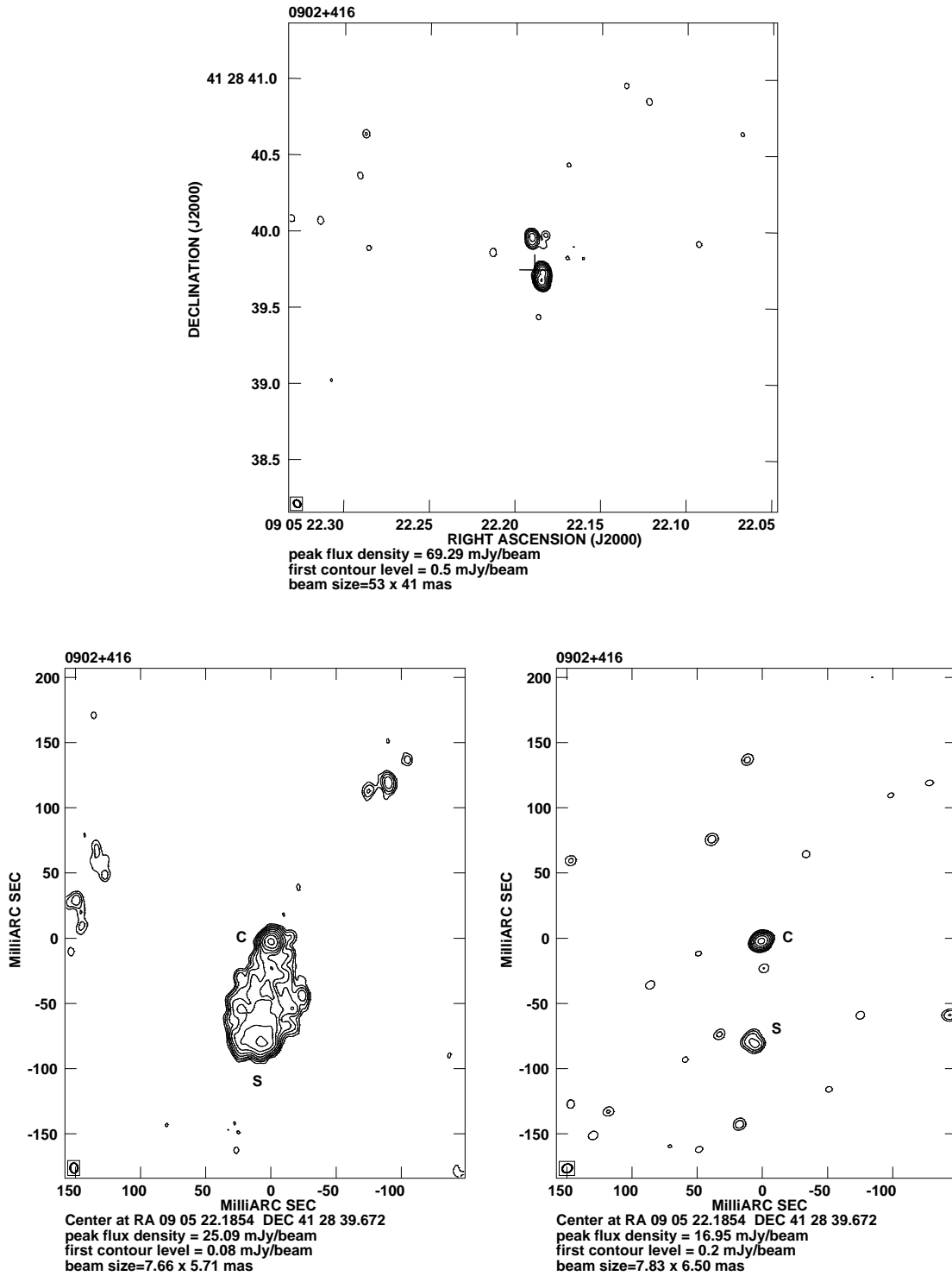


Fig. 8. 0902+416 — MERLIN map at 5 GHz (upper panel), VLBA map at 1.7 GHz (lower left panel) and EVN map at 5 GHz (lower right panel). The cross on the MERLIN map indicates the position of an optical object in SDSS/DR4.

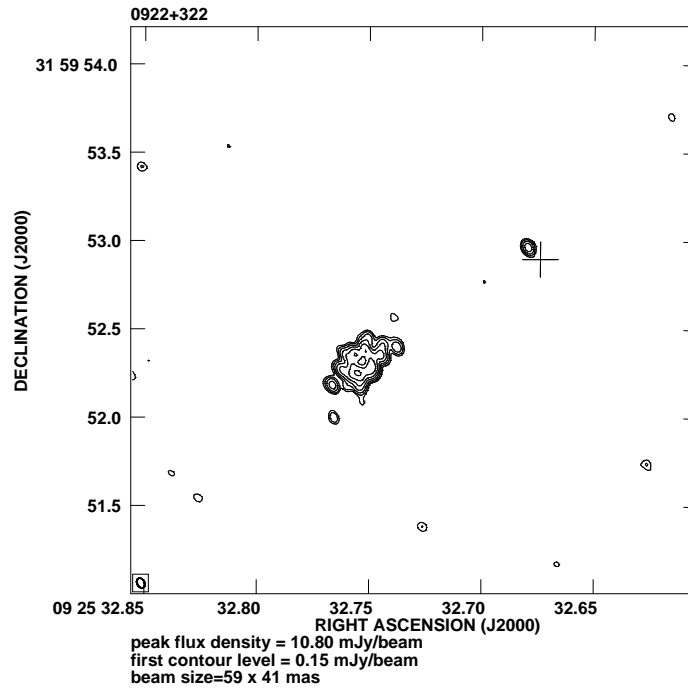


Fig. 9. MERLIN map of 0922+322 at 5 GHz. The cross on the MERLIN map indicates the position of an optical object in SDSS/DR4.

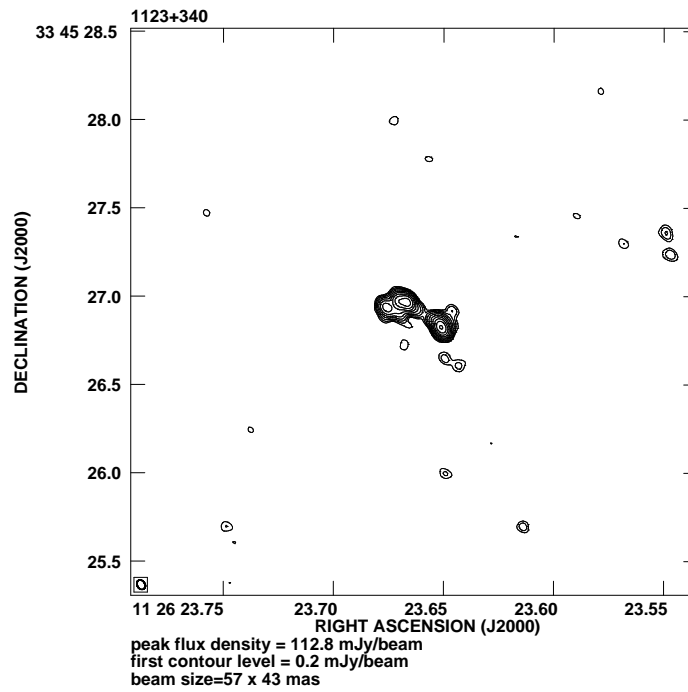


Fig. 10. 1123+340 — MERLIN map at 5 GHz.

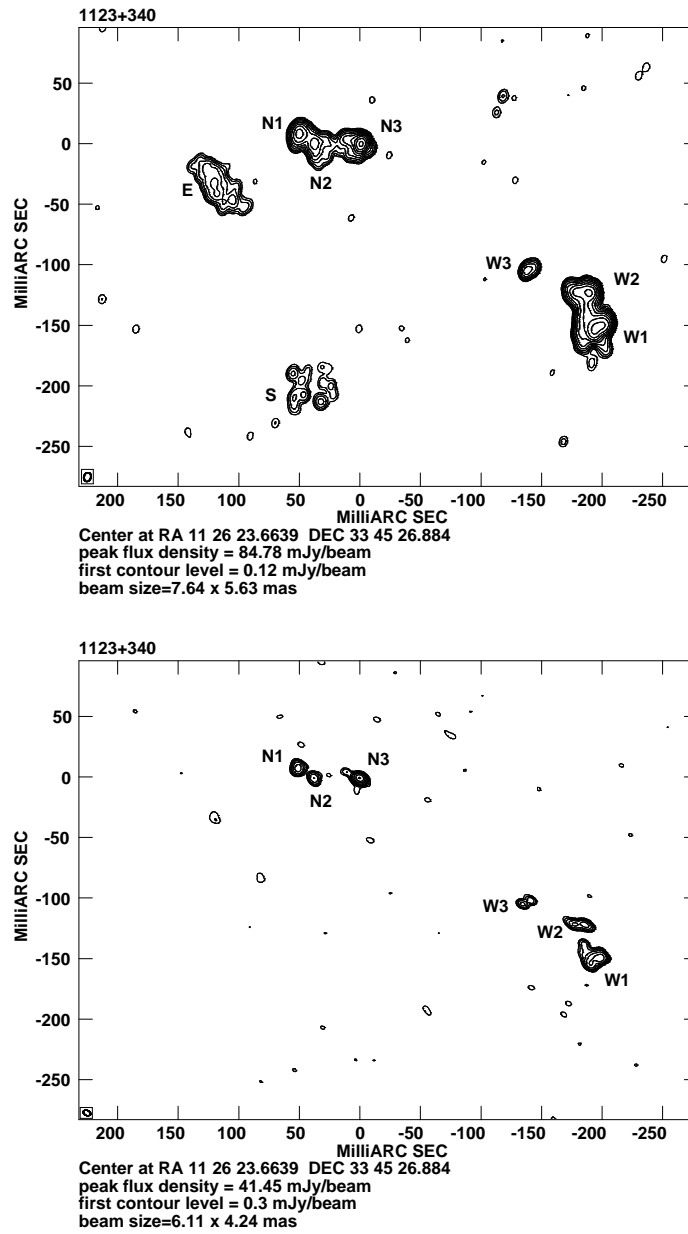


Fig. 10. (continued) 1123+340 — VLBA map at 1.7 GHz (upper panel) and EVN map at 5 GHz (lower panel).

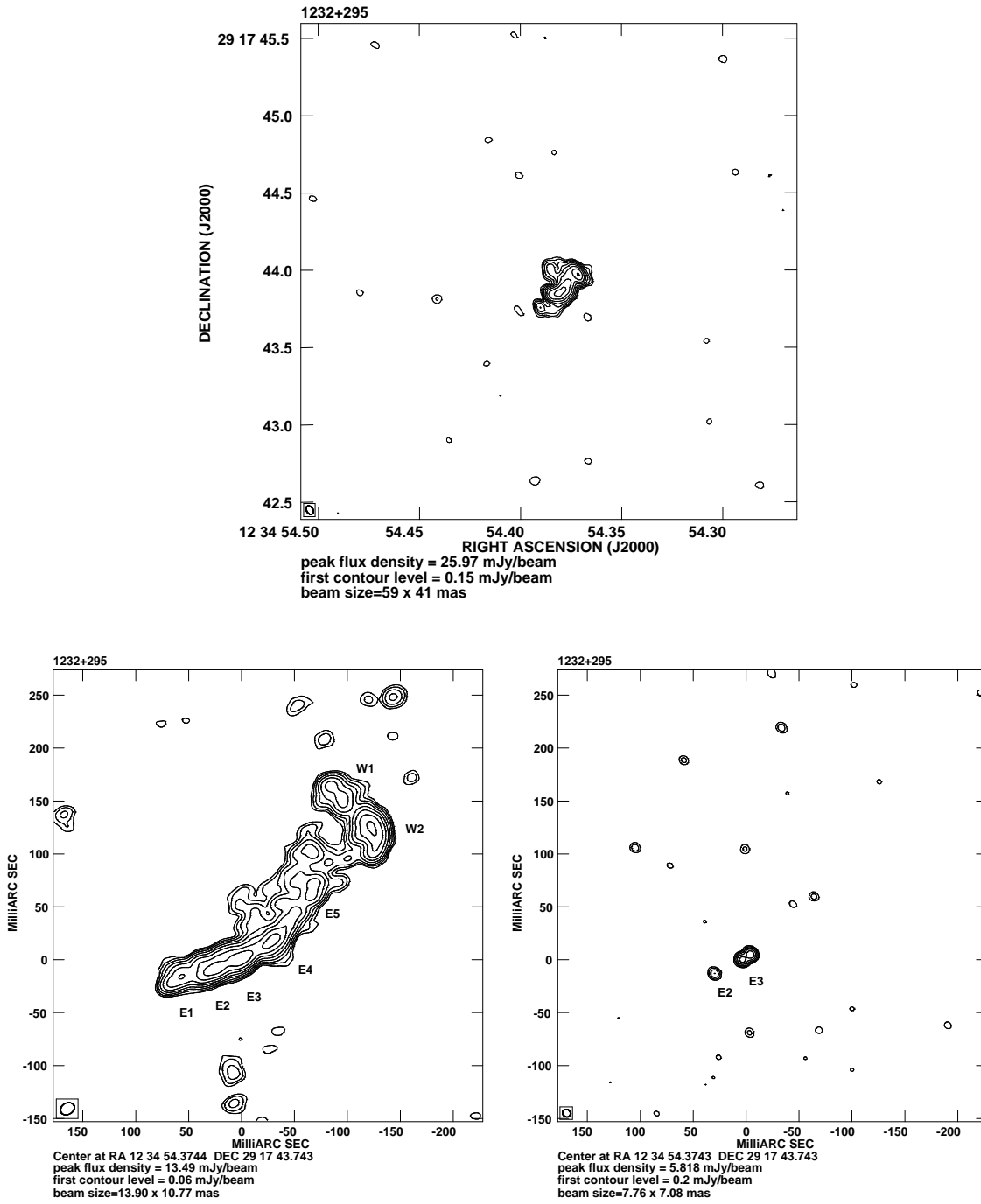


Fig. 11. 1232+295 – MERLIN map at 5 GHz (upper panel), VLBA map at 1.7 GHz (lower left panel) and EVN map at 5 GHz (lower right panel).

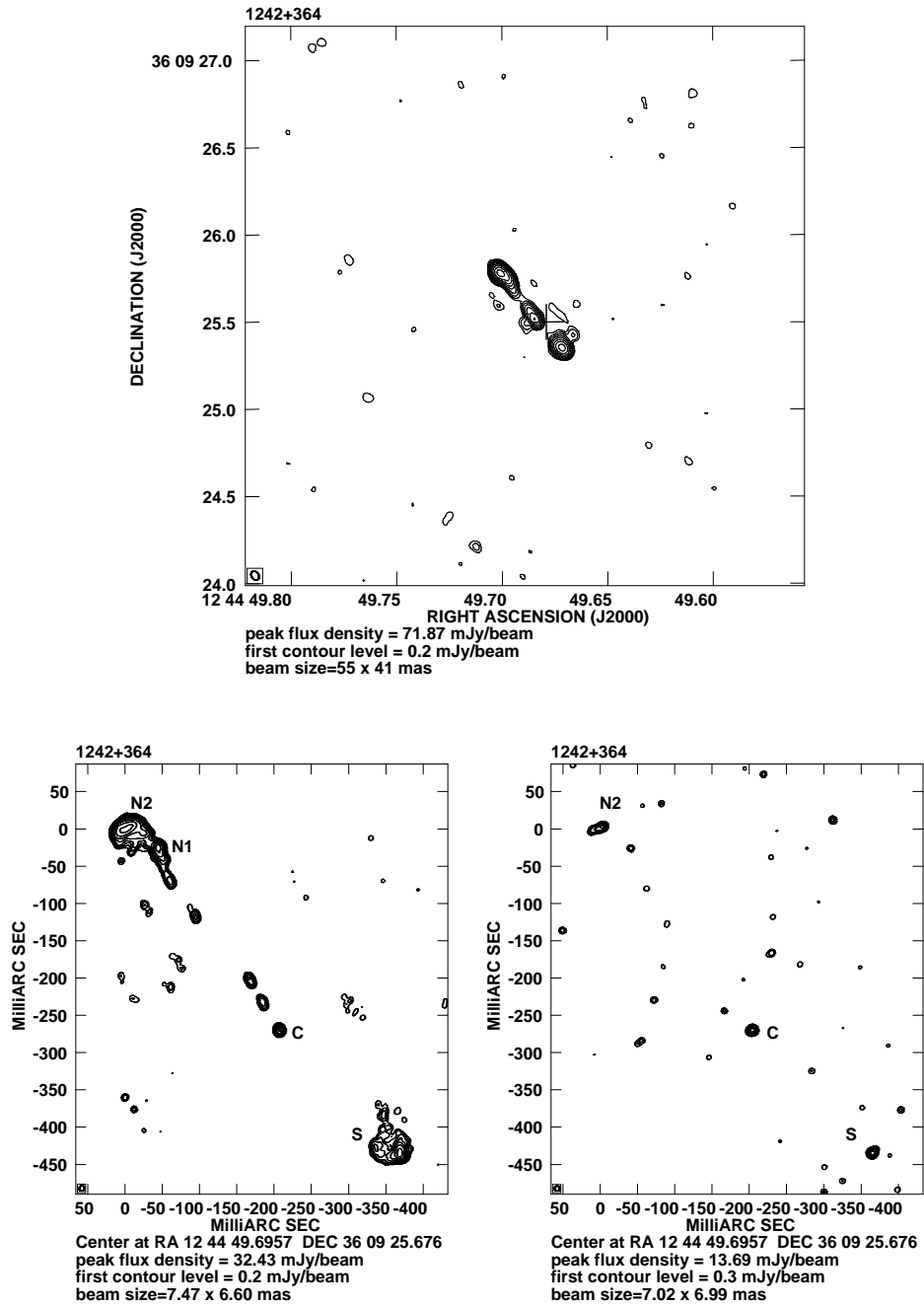


Fig. 12. 1242+364 – MERLIN map at 5 GHz (upper panel), VLBA map at 1.7 GHz (lower left panel) and EVN map at 5 GHz (lower right panel). The cross on the MERLIN map indicates the position of an optical object in SDSS/DR4.

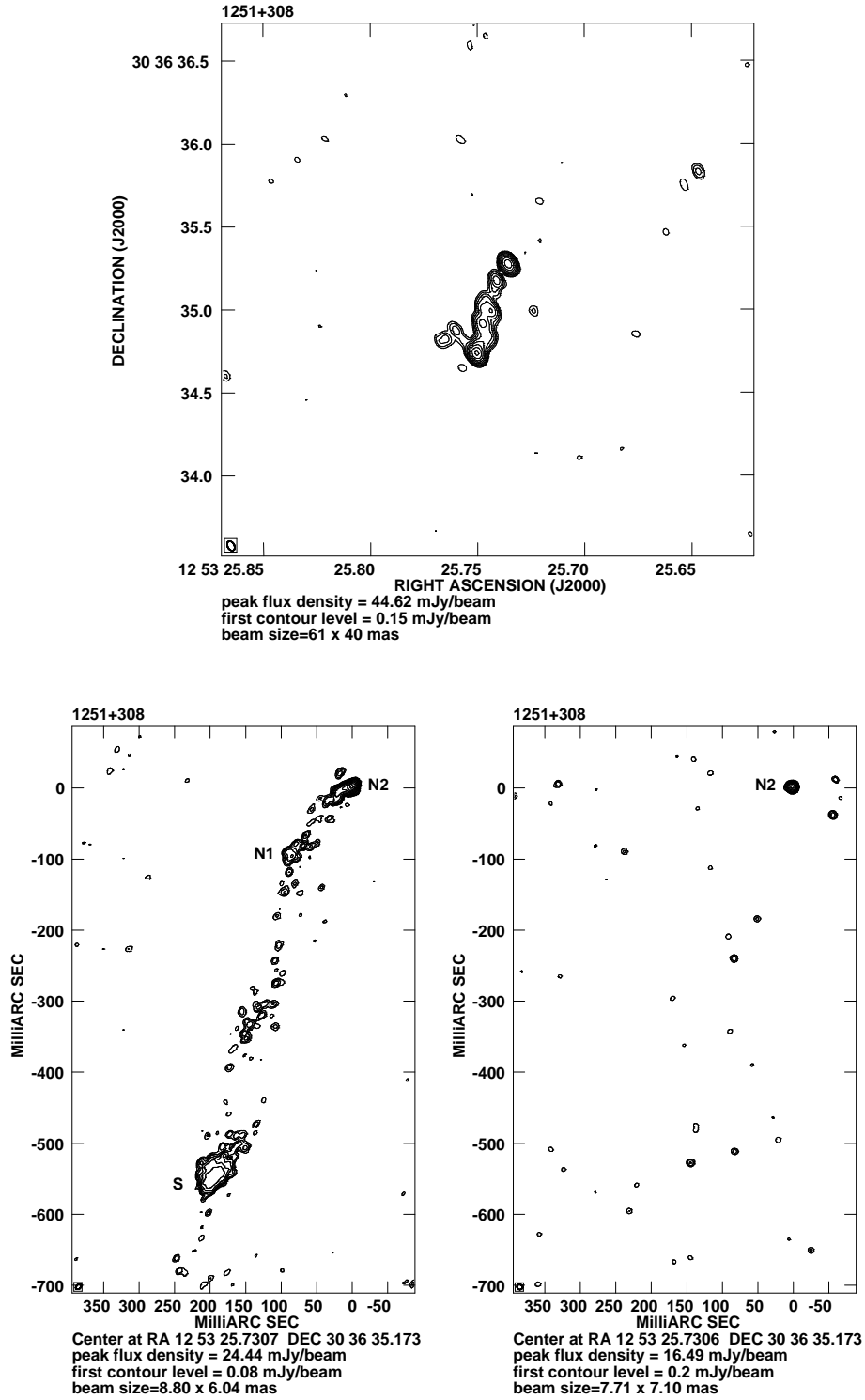


Fig. 13. 1251+308 – MERLIN map at 5 GHz (upper panel), VLBA map at 1.7 GHz (lower left panel) and EVN map at 5 GHz (lower right panel).

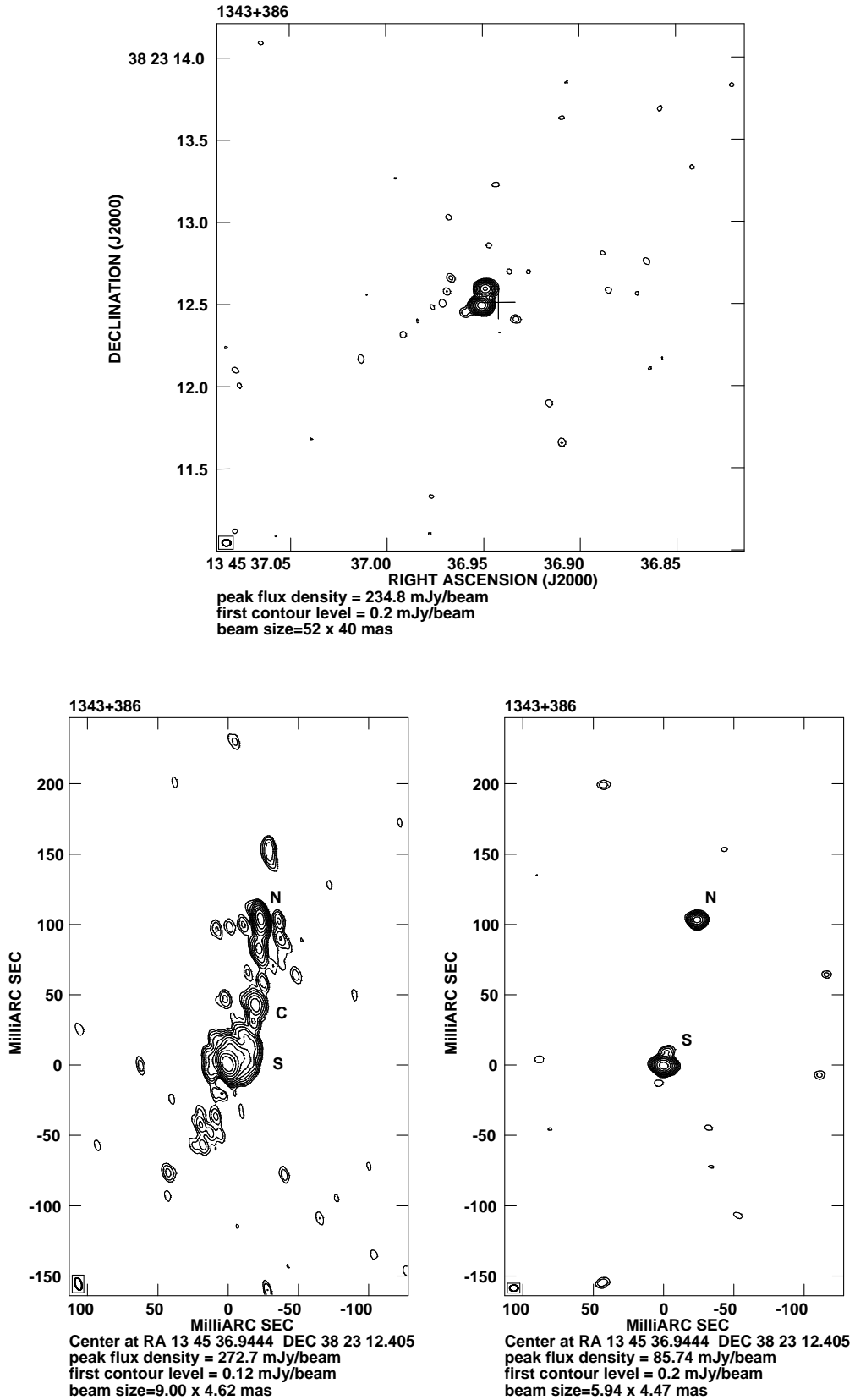


Fig. 14. 1343+386 – MERLIN map at 5 GHz (upper panel), VLBA map at 1.7 GHz (lower left panel) and EVN map at 5 GHz (lower right panel). The cross on the MERLIN map indicates the position of an optical object in SDSS/DR4.

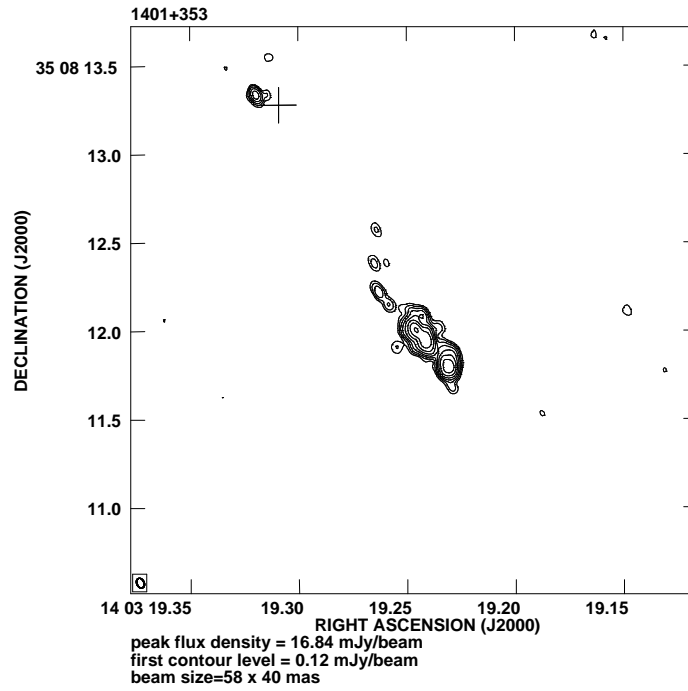


Fig. 15. MERLIN map of 1401+353 at 5 GHz. The cross on the MERLIN map indicates the position of an optical object in SDSS/DR4.

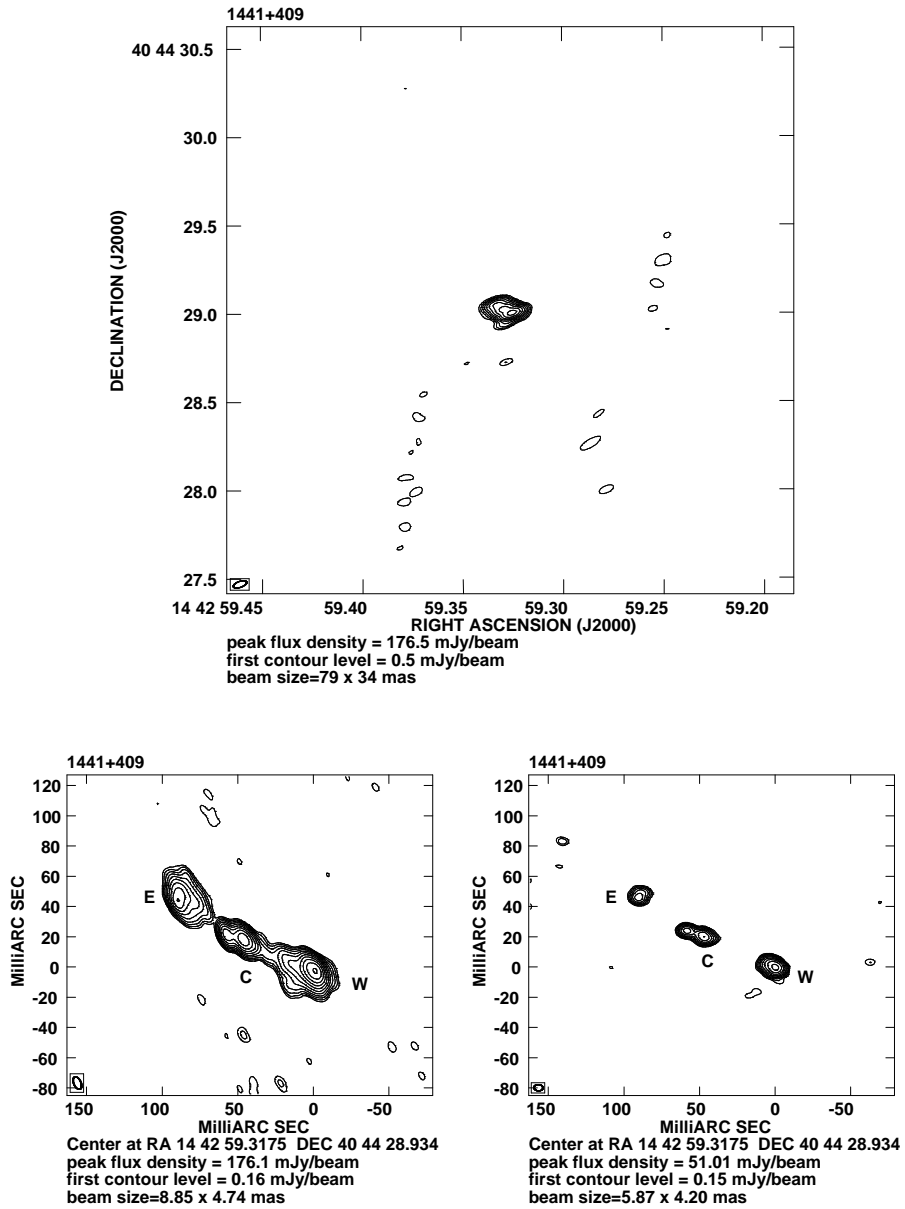


Fig. 16. 1441+409 – MERLIN map at 5 GHz (upper panel), VLBA map at 1.7 GHz (lower left panel) and EVN map at 5 GHz (lower right panel).

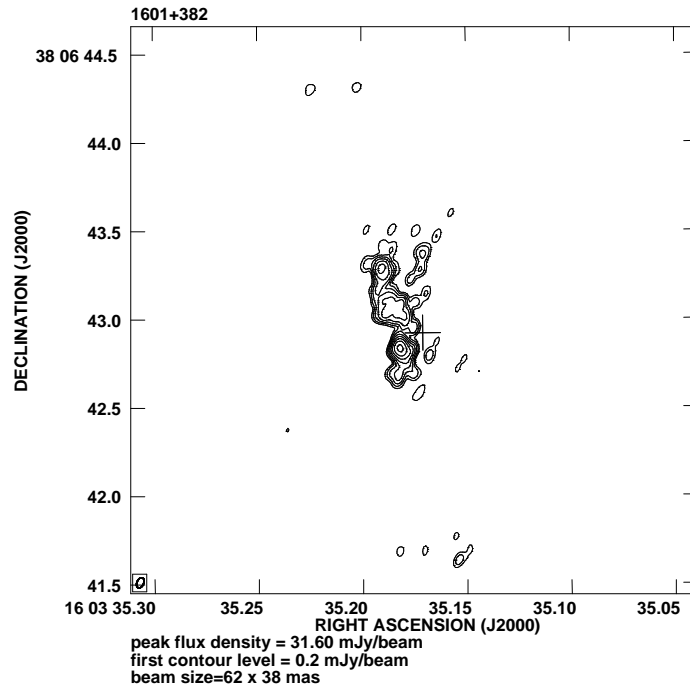


Fig. 17. MERLIN map of 1601+382 at 5 GHz. The cross on the MERLIN map indicates the position of an optical object in SDSS/DR4.

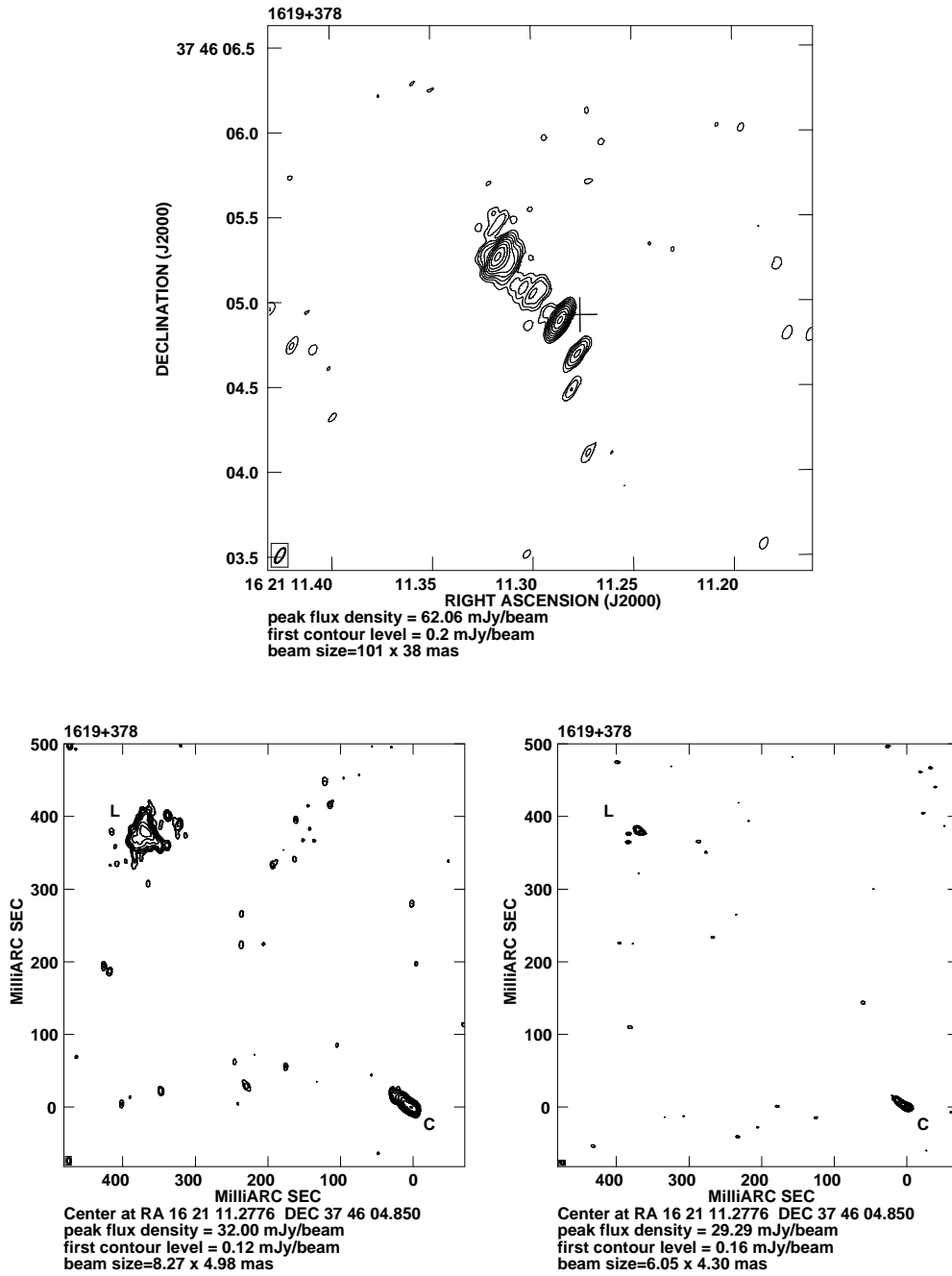


Fig. 18. 1619+378 – MERLIN map at 5 GHz (upper panel), VLBA map at 1.7 GHz (lower left panel) and EVN map at 5 GHz (lower right panel). The cross on the MERLIN map indicates the position of an optical object in SDSS/DR4.

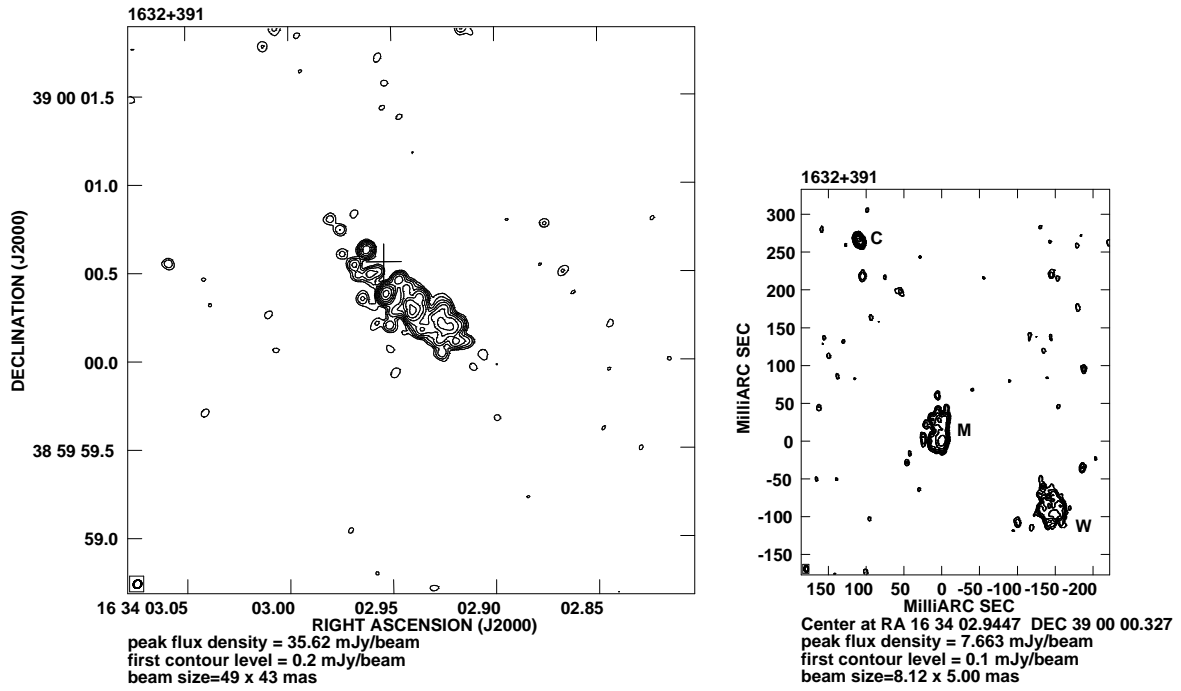


Fig. 19. 1632+391 – MERLIN map at 5 GHz (left panel) and VLBA map at 1.7 GHz (right panel). The cross on the MERLIN map indicates the position of an optical object in SDSS/DR4.

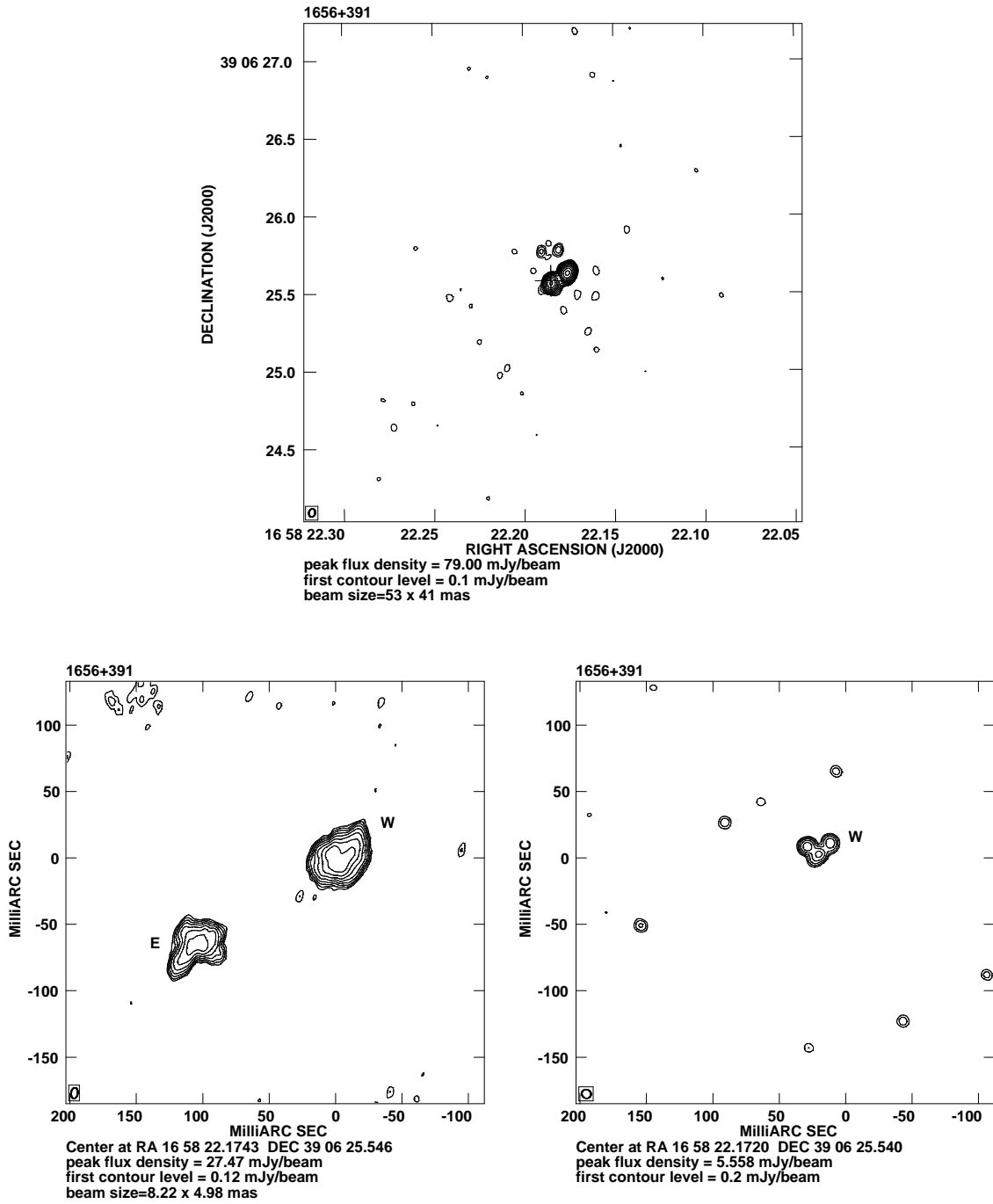


Fig. 20. 1656+391 – MERLIN map at 5 GHz (upper panel), VLBA map at 1.7 GHz (lower left panel) and EVN map at 5 GHz (lower right panel). The cross on the MERLIN map indicates the position of an optical object in SDSS/DR4.

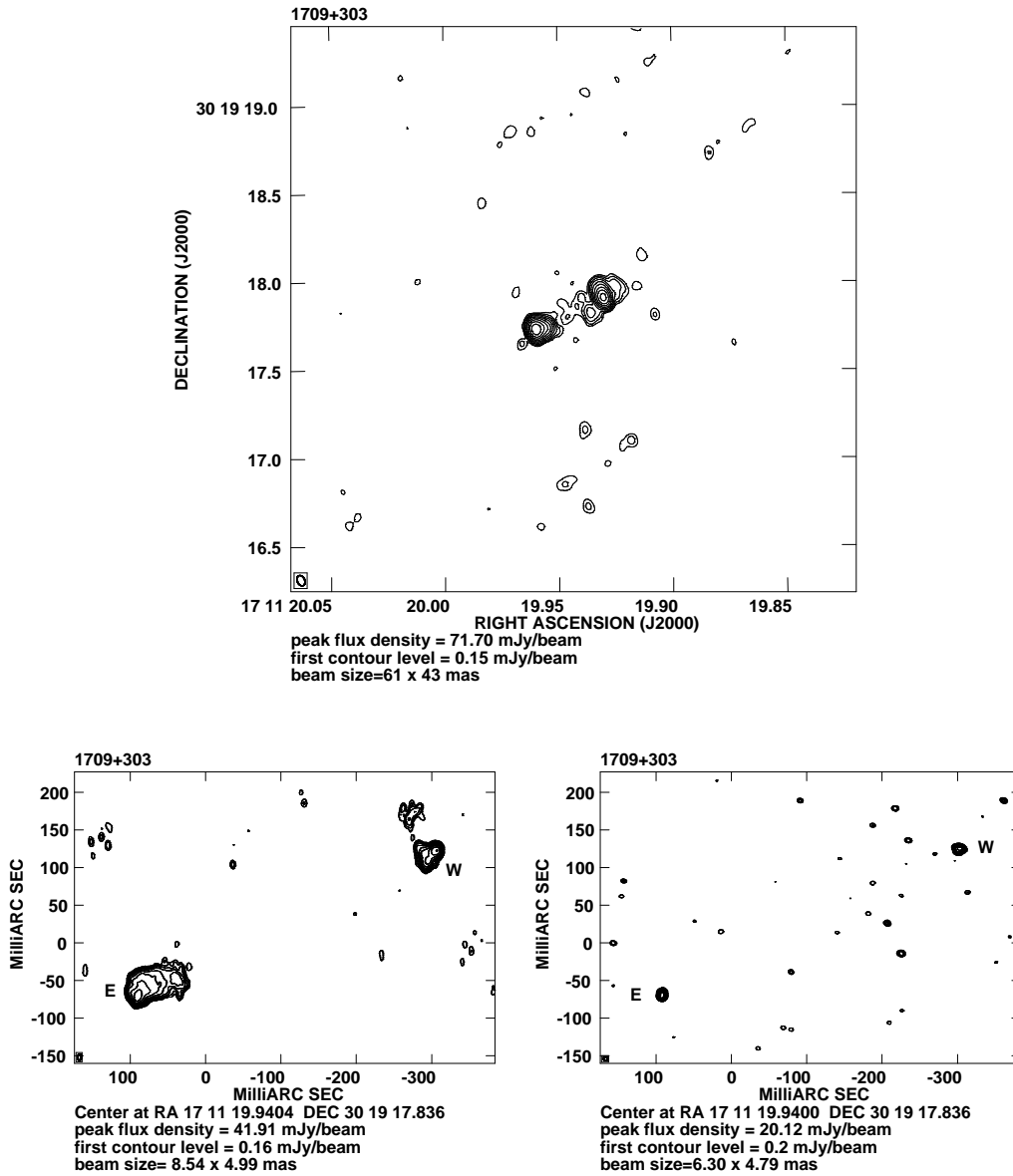


Fig. 21. 1709+303 – MERLIN map at 5 GHz (upper panel), VLBA map at 1.7 GHz (lower left panel) and EVN map at 5 GHz (lower right panel).

List of Objects

'0744+291' on page 5
'0747+314' on page 6
'0811+360' on page 6
'0853+291' on page 6
'0902+416' on page 6
'0922+322' on page 6
'1123+340' on page 7
'1232+295' on page 7
'1242+364' on page 7
'1251+308' on page 7
'1343+386' on page 7
'1401+353' on page 8
'1441+409' on page 8
'1601+382' on page 8
'1619+378' on page 8
'1632+391' on page 8
'1656+391' on page 8
'1709+303' on page 8
'1717+315' on page 9

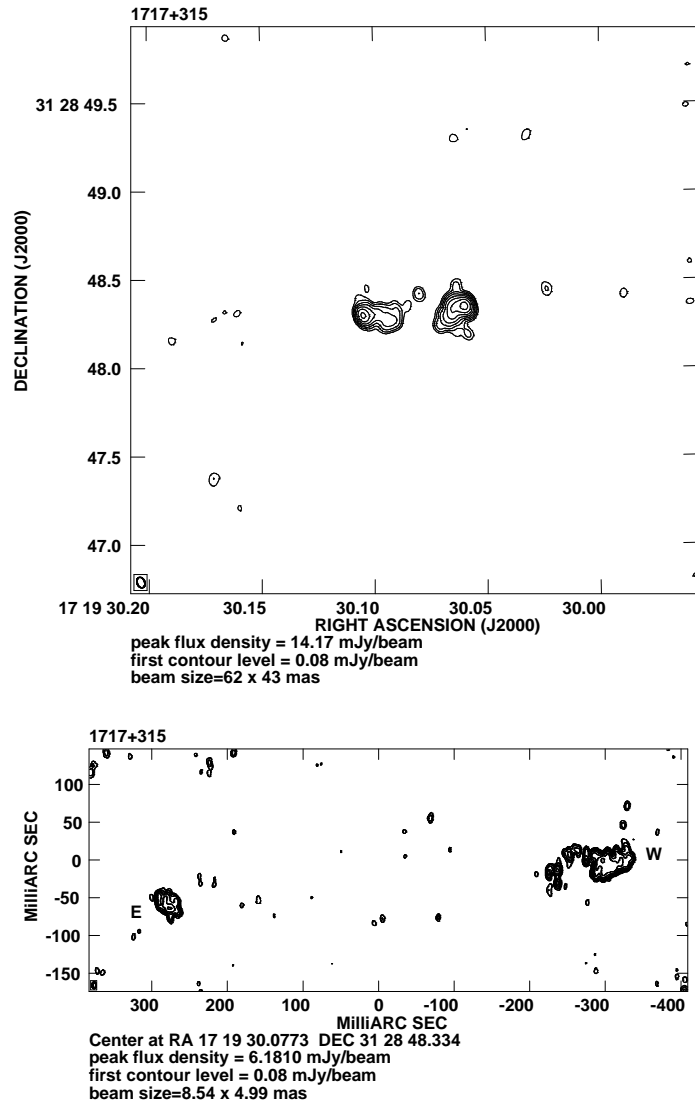


Fig. 22. 1717+315 – MERLIN map at 5 GHz (upper panel) and VLBA map at 1.7 GHz (lower panel).